Eur. Phys. J. C 14, 557–584 (2000)
Digital Object Identifier (DOI) 10.1007/s100520000354

THE EUROPEAN PHYSICAL JOURNAL C

Consistent measurements of α_s from precise oriented event shape distributions

The DELPHI Collaboration

P.Abreu[22], W.Adam[52], T.Adye[38], P.Adzic[12], Z.Albrecht[18], T.Alderweireld[2], G.D.Alekseev[17], R.Alemany[51], T.Allmendinger[18], P.P.Allport[23], S.Almehed[25], U.Amaldi[29], N.Amapane[47], S.Amato[49], E.G.Anassontzis[3], P.Andersson[46], A.Andreazza[9], S.Andringa[22], P.Antilogus[26], W-D.Apel[18], Y.Arnoud[9], B.Åsman[46], J-E.Augustin[26], A.Augustinus[9], P.Baillon[9], P.Bambade[20], F.Barao[22], G.Barbiellini[48], R.Barbier[26], D.Y.Bardin[17], G.Barker[18], A.Baroncelli[40], M.Battaglia[16], M.Baubillier[24], K-H.Becks[54], M.Begalli[6], A.Behrmann[54], P.Beilliere[8], Yu.Belokopytov[9],55 N.C.Benekos[33], A.C.Benvenuti[5], C.Berat[15], M.Berggren[26], D.Bertini[26], D.Bertrand[2], M.Besancon[41], M.Bigi[47], M.S.Bilenky[17], M-A.Bizouard[20], D.Bloch[10], H.M.Blom[32], M.Bonesini[28], M.Boonekamp[41], P.S.L.Booth[23], A.W.Borgland[4], G.Borisov[20], C.Bosio[43], O.Botner[50], E.Boudinov[32], B.Bouquet[20], C.Bourdarios[20], T.J.V.Bowcock[23], I.Boyko[17], I.Bozovic[12], M.Bozzo[14], P.Branchini[40], T.Brenke[54], R.A.Brenner[50], P.Bruckman[19], J-M.Brunet[8], L.Bugge[34], T.Buran[34], T.Burgsmueller[54], B.Buschbeck[52], P.Buschmann[54], S.Cabrera[51], M.Caccia[28], M.Calvi[29], T.Camporesi[9], V.Canale[39], F.Carena[9], L.Carroll[23], C.Caso[14], M.V.Castillo Gimenez[51], A.Cattai[9], F.R.Cavallo[5], V.Chabaud[9], Ph.Charpentier[9], L.Chaussard[26], P.Checchia[37], G.A.Chelkov[17], R.Chierici[47], P.Chochula[7], V.Chorowicz[26], J.Chudoba[31], K.Cieslik[19], P.Collins[9], R.Contri[14], E.Cortina[51], G.Cosme[20], F.Cossutti[9], J-H.Cowell[23], H.B.Crawley[1], D.Crennell[38], S.Crepe[15], G.Crosetti[14], J.Cuevas Maestro[35], S.Czellar[16], M.Davenport[9], W.Da Silva[24], A.Deghorain[2], G.Della Ricca[48], P.Delpierre[27], N.Demaria[9], A.De Angelis[9], W.De Boer[18], C.De Clercq[2], B.De Lotto[48], A.De Min[37],9 L.De Paula[49], H.Dijkstra[9], L.Di Ciaccio[39],9 J.Dolbeau[8], K.Doroba[53], M.Dracos[10], J.Drees[54], M.Dris[33], A.Duperrin[26], J-D.Durand[9], G.Eigen[4], T.Ekelof[50], G.Ekspong[46], M.Ellert[50], M.Elsing[9], J-P.Engel[10], B.Erzen[45], M.Espirito Santo[22], G.Fanourakis[12], D.Fassouliotis[12], J.Fayot[24], M.Feindt[18], A.Ferrer[51], E.Ferrer-Ribas[20], F.Ferro[14], S.Fichet[24], A.Firestone[1], U.Flagmeyer[54], H.Foeth[9], E.Fokitis[33], F.Fontanelli[14], B.Franek[38], A.G.Frodesen[4], R.Fruhwirth[52], F.Fulda-Quenzer[20], J.Fuster[51], A.Galloni[23], D.Gamba[47], S.Gamblin[20], M.Gandelman[49], C.Garcia[51], C.Gaspar[9], M.Gaspar[49], U.Gasparini[37], Ph.Gavillet[9], E.N.Gazis[33], D.Gele[10], N.Ghodbane[26], I.Gil[51], F.Glege[54], R.Gokieli[9],53 B.Golob[45], G.Gomez-Ceballos[42], P.Goncalves[22], I.Gonzalez Caballero[42], G.Gopal[38], L.Gorn[1],56 V.Gracco[14], J.Grahl[1], E.Graziani[40], C.Green[23], H-J.Grimm[18], P.Gris[41], G.Grosdidier[20], K.Grzelak[53], M.Gunther[50], J.Guy[38], F.Hahn[9], S.Hahn[54], S.Haider[9], A.Hallgren[50], K.Hamacher[54], J.Hansen[34], F.J.Harris[36], V.Hedberg[25], S.Heising[18], J.J.Hernandez[51], P.Herquet[2], H.Herr[9], T.L.Hessing[36], J.-M.Heuser[54], E.Higon[51], S-O.Holmgren[46], P.J.Holt[36], S.Hoorelbeke[2], M.Houlden[23], J.Hrubec[52], K.Huet[2], G.J.Hughes[23], K.Hultqvist[46], J.N.Jackson[23], R.Jacobsson[9], P.Jalocha[9], R.Janik[7], Ch.Jarlskog[25], G.Jarlskog[25], P.Jarry[41], B.Jean-Marie[20], E.K.Johansson[46], P.Jonsson[26], C.Joram[9], P.Juillot[10], F.Kapusta[24], K.Karafasoulis[12], S.Katsanevas[26], E.C.Katsoufis[33], R.Keranen[18], B.P.Kersevan[45], B.A.Khomenko[17], N.N.Khovanski[17], A.Kiiskinen[16], B.King[23], A.Kinvig[23], N.J.Kjaer[32], O.Klapp[54], H.Klein[9], P.Kluit[32], P.Kokkinias[12], M.Koratzinos[9], C.Kourkoumelis[3], O.Kouznetsov[41], M.Krammer[52], E.Kriznic[45], Z.Krumstein[17], P.Kubinec[7], J.Kurowska[53], K.Kurvinen[16], J.W.Lamsa[1], D.W.Lane[1], P.Langefeld[54], J-P.Laugier[41], R.Lauhakangas[16], G.Leder[52], F.Ledroit[15], V.Lefebure[2], L.Leinonen[46], A.Leisos[12], R.Leitner[31], J.Lemonne[2], G.Lenzen[54], V.Lepeltier[20], T.Lesiak[19], M.Lethuillier[41], J.Libby[36], D.Liko[9], A.Lipniacka[46], I.Lippi[37], B.Loerstad[25], J.G.Loken[36], J.H.Lopes[49], J.M.Lopez[42], R.Lopez-Fernandez[15], D.Loukas[12], P.Lutz[41], L.Lyons[36], J.MacNaughton[52], J.R.Mahon[6], A.Maio[22], A.Malek[54], T.G.M.Malmgren[46], S.Maltezos[33], V.Malychev[17], F.Mandl[52], J.Marco[42], R.Marco[42], B.Marechal[49], M.Margoni[37], J-C.Marin[9], C.Mariotti[9], A.Markou[12], C.Martinez-Rivero[20], F.Martinez-Vidal[51], S.Marti i Garcia[9], J.Masik[13], N.Mastroyiannopoulos[12], F.Matorras[42], C.Matteuzzi[29], G.Matthiae[39], F.Mazzucato[37], M.Mazzucato[37], M.Mc Cubbin[23], R.Mc Kay[1], R.Mc Nulty[23], G.Mc Pherson[23], C.Meroni[28], W.T.Meyer[1], E.Migliore[47], L.Mirabito[26], W.A.Mitaroff[52], U.Mjoernmark[25], T.Moa[46], M.Moch[18], R.Moeller[30], K.Moenig[9], M.R.Monge[14], X.Moreau[24], P.Morettini[14], G.Morton[36], U.Mueller[54], K.Muenich[54], M.Mulders[32], C.Mulet-Marquis[15], R.Muresan[25], W.J.Murray[38], B.Muryn[15],19 G.Myatt[36], T.Myklebust[34], F.Naraghi[15], M.Nassiakou[12], F.L.Navarria[5], S.Navas[51], K.Nawrocki[53], P.Negri[29], S.Nemecek[13], N.Neufeld[9], R.Nicolaidou[41], B.S.Nielsen[30], P.Niezurawski[53], M.Nikolenko[10],17 V.Nomokonov[16], A.Normand[23], A.Nygren[25], A.G.Olshevski[17], A.Onofre[22], R.Orava[16], G.Orazi[10], K.Osterberg[16], A.Ouraou[41], M.Paganoni[29], S.Paiano[5], R.Pain[24], R.Paiva[22], J.Palacios[36], H.Palka[19], Th.D.Papadopoulou[33],9 K.Papageorgiou[12], L.Pape[9], C.Parkes[9], F.Parodi[14], U.Parzefall[23], A.Passeri[40], O.Passon[54], M.Pegoraro[37], L.Peralta[22], M.Pernicka[52], A.Perrotta[5], C.Petridou[48], A.Petrolini[14], H.T.Phillips[38], F.Pierre[41], M.Pimenta[22], E.Piotto[28], T.Podobnik[45], M.E.Pol[6], G.Polok[19],

P.Poropat[48], V.Pozdniakov[17], P.Privitera[39], N.Pukhaeva[17], A.Pullia[29], D.Radojicic[36], S.Ragazzi[29], H.Rahmani[33], P.N.Ratoff[21], A.L.Read[34], P.Rebecchi[9], N.G.Redaelli[29], M.Regler[52], D.Reid[32], R.Reinhardt[54], P.B.Renton[36], L.K.Resvanis[3], F.Richard[20], J.Ridky[13], G.Rinaudo[47], G.Rodrigo, O.Rohne[34], A.Romero[47], P.Ronchese[37], E.I.Rosenberg[1], P.Rosinsky[7], P.Roudeau[20], T.Rovelli[5], Ch.Royon[41], V.Ruhlmann-Kleider[41], A.Ruiz[42], H.Saarikko[16], Y.Sacquin[41], A.Sadovsky[17], G.Sajot[15], J.Salt[51], D.Sampsonidis[12], M.Sannino[14], H.Schneider[18], Ph.Schwemling[24], B.Schwering[54], U.Schwickerath[18], M.A.E.Schyns[54], F.Scuri[48], P.Seager[21], Y.Sedykh[17], A.M.Segar[36], R.Sekulin[38], R.C.Shellard[6], A.Sheridan[23], M.Siebel[54], L.Simard[41], F.Simonetto[37], A.N.Sisakian[17], G.Smadja[26], O.Smirnova[25], G.R.Smith[38], A.Sopczak[18], R.Sosnowski[53], T.Spassov[22], E.Spiriti[40], P.Sponholz[54], S.Squarcia[14], C.Stanescu[40], S.Stanic[45], K.Stevenson[36], A.Stocchi[20], J.Strauss[52], R.Strub[10], B.Stugu[4], M.Szczekowski[53], M.Szeptycka[53], T.Tabarelli[29], F.Tegenfeldt[50], F.Terranova[28], J.Thomas[36], J.Timmermans[32], N.Tinti[5], L.G.Tkatchev[17], S.Todorova[10], A.Tomaradze[2], B.Tome[22], A.Tonazzo[9], L.Tortora[40], G.Transtromer[25], D.Treille[9], G.Tristram[8], M.Trochimczuk[53], C.Troncon[28], A.Tsirou[9], M-L.Turluer[41], I.A.Tyapkin[17], S.Tzamarias[12], O.Ullaland[9], G.Valenti[5], E.Vallazza[48], C.Vander Velde[2], G.W.Van Apeldoorn[32], P.Van Dam[32], W.K.Van Doninck[2], J.Van Eldik[32], A.Van Lysebetten[2], N.Van Remortel[2], I.Van Vulpen[32], N.Vassilopoulos[36], G.Vegni[28], L.Ventura[37], W.Venus[38],9 F.Verbeure[2], M.Verlato[37], L.S.Vertogradov[17], V.Verzi[39], D.Vilanova[41], L.Vitale[48], A.S.Vodopyanov[17], C.Vollmer[18], G.Voulgaris[3], V.Vrba[13], H.Wahlen[54], C.Walck[46], C.Weiser[18], D.Wicke[54], J.H.Wickens[2], G.R.Wilkinson[9], M.Winter[10], M.Witek[19], G.Wolf[9], J.Yi[1], A.Zalewska[19], P.Zalewski[53], D.Zavrtanik[45], E.Zevgolatakos[12], N.I.Zimin[17],25 G.C.Zucchelli[46], G.Zumerle[37]

[1] Department of Physics and Astronomy, Iowa State University, Ames IA 50011-3160, USA
[2] Physics Department, Univ. Instelling Antwerpen, Universiteitsplein 1, 2610 Antwerpen, Belgium
and IIHE, ULB-VUB, Pleinlaan 2, 1050 Brussels, Belgium
and Faculté des Sciences, Univ. de l'Etat Mons, Av. Maistriau 19, 7000 Mons, Belgium
[3] Physics Laboratory, University of Athens, Solonos Str. 104, 10680 Athens, Greece
[4] Department of Physics, University of Bergen, Allégaten 55, 5007 Bergen, Norway
[5] Dipartimento di Fisica, Università di Bologna and INFN, Via Irnerio 46, 40126 Bologna, Italy
[6] Centro Brasileiro de Pesquisas Físicas, rua Xavier Sigaud 150, 22290 Rio de Janeiro, Brazil
and Depto. de Física, Pont. Univ. Católica, C.P. 38071 22453 Rio de Janeiro, Brazil
and Inst. de Física, Univ. Estadual do Rio de Janeiro, rua São Francisco Xavier 524, Rio de Janeiro, Brazil
[7] Comenius University, Faculty of Mathematics and Physics, Mlynska Dolina, 84215 Bratislava, Slovakia
[8] Collège de France, Lab. de Physique Corpusculaire, IN2P3-CNRS, 75231 Paris Cedex 05, France
[9] CERN, 1211 Geneva 23, Switzerland
[10] Institut de Recherches Subatomiques, IN2P3 - CNRS/ULP - BP20, 67037 Strasbourg Cedex, France
[11] Now at DESY-Zeuthen, Platanenallee 6, 15735 Zeuthen, Germany
[12] Institute of Nuclear Physics, N.C.S.R. Demokritos, P.O. Box 60228, 15310 Athens, Greece
[13] FZU, Inst. of Phys. of the C.A.S. High Energy Physics Division, Na Slovance 2, 180 40, Praha 8, Czech Republic
[14] Dipartimento di Fisica, Università di Genova and INFN, Via Dodecaneso 33, 16146 Genova, Italy
[15] Institut des Sciences Nucléaires, IN2P3-CNRS, Université de Grenoble 1, 38026 Grenoble Cedex, France
[16] Helsinki Institute of Physics, HIP, P.O. Box 9, 00014 Helsinki, Finland
[17] Joint Institute for Nuclear Research, Dubna, Head Post Office, P.O. Box 79, 101 000 Moscow, Russian Federation
[18] Institut für Experimentelle Kernphysik, Universität Karlsruhe, Postfach 6980, 76128 Karlsruhe, Germany
[19] Institute of Nuclear Physics and University of Mining and Metalurgy, Ul. Kawiory 26a, 30055 Krakow, Poland
[20] Université de Paris-Sud, Lab. de l'Accélérateur Linéaire, IN2P3-CNRS, Bât. 200, 91405 Orsay Cedex, France
[21] School of Physics and Chemistry, University of Lancaster, Lancaster LA1 4YB, UK
[22] LIP, IST, FCUL - Av. Elias Garcia, 14-1^o, 1000 Lisboa Codex, Portugal
[23] Department of Physics, University of Liverpool, P.O. Box 147, Liverpool L69 3BX, UK
[24] LPNHE, IN2P3-CNRS, Univ. Paris VI et VII, Tour 33 (RdC), 4 place Jussieu, 75252 Paris Cedex 05, France
[25] Department of Physics, University of Lund, Sölvegatan 14, 223 63 Lund, Sweden
[26] Université Claude Bernard de Lyon, IPNL, IN2P3-CNRS, 69622 Villeurbanne Cedex, France
[27] Univ. d'Aix - Marseille II - CPP, IN2P3-CNRS, 13288 Marseille Cedex 09, France
[28] Dipartimento di Fisica, Università di Milano and INFN, Via Celoria 16, 20133 Milan, Italy
[29] Università degli Studi di Milano - Bicocca, Via Emanuelli 15, 20126 Milan, Italy
[30] Niels Bohr Institute, Blegdamsvej 17, 2100 Copenhagen Ø, Denmark
[31] IPNP of MFF, Charles Univ., Areal MFF, V Holesovickach 2, 180 00, Praha 8, Czech Republic
[32] NIKHEF, Postbus 41882, 1009 DB Amsterdam, The Netherlands
[33] National Technical University, Physics Department, Zografou Campus, 15773 Athens, Greece
[34] Physics Department, University of Oslo, Blindern, 1000 Oslo 3, Norway
[35] Dpto. Fisica, Univ. Oviedo, Avda. Calvo Sotelo s/n, 33007 Oviedo, Spain
[36] Department of Physics, University of Oxford, Keble Road, Oxford OX1 3RH, UK
[37] Dipartimento di Fisica, Università di Padova and INFN, Via Marzolo 8, 35131 Padua, Italy
[38] Rutherford Appleton Laboratory, Chilton, Didcot OX11 OQX, UK
[39] Dipartimento di Fisica, Università di Roma II and INFN, Tor Vergata, 00173 Rome, Italy

[40] Dipartimento di Fisica, Università di Roma III and INFN, Via della Vasca Navale 84, 00146 Rome, Italy
[41] DAPNIA/Service de Physique des Particules, CEA-Saclay, 91191 Gif-sur-Yvette Cedex, France
[42] Instituto de Fisica de Cantabria (CSIC-UC), Avda. los Castros s/n, 39006 Santander, Spain
[43] Dipartimento di Fisica, Università degli Studi di Roma La Sapienza, Piazzale Aldo Moro 2, 00185 Rome, Italy
[44] Inst. for High Energy Physics, Serpukov P.O. Box 35, Protvino, (Moscow Region), Russian Federation
[45] J. Stefan Institute, Jamova 39, 1000 Ljubljana, Slovenia and Laboratory for Astroparticle Physics, Nova Gorica Polytechnic, Kostanjeviska 16a, 5000 Nova Gorica, Slovenia, and Department of Physics, University of Ljubljana, 1000 Ljubljana, Slovenia
[46] Fysikum, Stockholm University, Box 6730, 113 85 Stockholm, Sweden
[47] Dipartimento di Fisica Sperimentale, Università di Torino and INFN, Via P. Giuria 1, 10125 Turin, Italy
[48] Dipartimento di Fisica, Università di Trieste and INFN, Via A. Valerio 2, 34127 Trieste, Italy and Istituto di Fisica, Università di Udine, 33100 Udine, Italy
[49] Univ. Federal do Rio de Janeiro, C.P. 68528 Cidade Univ., Ilha do Fundão 21945-970 Rio de Janeiro, Brazil
[50] Department of Radiation Sciences, University of Uppsala, P.O. Box 535, 751 21 Uppsala, Sweden
[51] IFIC, Valencia-CSIC, and D.F.A.M.N., U. de Valencia, Avda. Dr. Moliner 50, 46100 Burjassot (Valencia), Spain
[52] Institut für Hochenergiephysik, Österr. Akad. d. Wissensch., Nikolsdorfergasse 18, 1050 Vienna, Austria
[53] Inst. Nuclear Studies and University of Warsaw, Ul. Hoza 69, 00681 Warsaw, Poland
[54] Fachbereich Physik, University of Wuppertal, Postfach 100 127, 42097 Wuppertal, Germany
[55] On leave of absence from IHEP Serpukhov
[56] Now at University of Florida

Received: 8 October 1999 / Revised version: 26 January 2000 /
Published online: 18 May 2000 –

Abstract. An updated analysis using about 1.5 million events recorded at $\sqrt{s} = M_Z$ with the DELPHI detector in 1994 is presented. Eighteen infrared and collinear safe event shape observables are measured as a function of the polar angle of the thrust axis. The data are compared to theoretical calculations in $\mathcal{O}(\alpha_s^2)$ including the event orientation. A combined fit of α_s and of the renormalization scale x_μ in $\mathcal{O}(\alpha_s^2)$ yields an excellent description of the high statistics data.

The weighted average from 18 observables including quark mass effects and correlations is $\alpha_s(M_Z^2) = 0.1174 \pm 0.0026$. The final result, derived from the jet cone energy fraction, the observable with the smallest theoretical and experimental uncertainty, is

$$\alpha_s(M_Z^2) = 0.1180 \pm 0.0006(\text{exp.}) \pm 0.0013(\text{hadr.}) \pm 0.0008(\text{scale}) \pm 0.0007(\text{mass}).$$

Further studies include an α_s determination using theoretical predictions in the next-to-leading log approximation (NLLA), matched NLLA and $\mathcal{O}(\alpha_s^2)$ predictions as well as theoretically motivated optimized scale setting methods. The influence of higher order contributions was also investigated by using the method of Padé approximants. Average α_s values derived from the different approaches are in good agreement.

1 Introduction

This paper presents a highly improved test of second order perturbation theory and an improved measurement of $\alpha_s(M_Z^2)$. It is based on progress in next-to-leading order QCD calculations of oriented event shape distributions [1]. Furthermore, the DELPHI data used in this analysis are much improved in both their statistical and systematic precision compared with those of previous DELPHI publications [2,3]. The distributions of 18 different infrared and collinear safe hadronic event observables are determined from 1.4 million hadronic Z-decays at various values of the polar angle ϑ_T of the thrust axis. The ϑ_T dependence of all detector properties are taken into account, thus achieving the best possible experimental precision.

The precise experimental data are fully consistent with the expectation from second order QCD. A two parameter fit to each of the distributions measured at different polar angles ϑ_T allows an experimental optimization of the $\mathcal{O}(\alpha_s^2)$ renormalization scale giving a consistent set of eighteen $\alpha_s(M_Z^2)$ values. For most of the distributions the largest uncertainty on the $\alpha_s(M_Z^2)$ values is due to hadronization corrections and not to renormalization scale errors. Any artificial increase [4] of the uncertainty of $\alpha_s(M_Z^2)$ due to a large variation of the renormalization scale is avoided so that the degree of precision to which QCD can be tested remains transparent. An average value of $\alpha_s(M_Z^2)$ is derived taking account of the correlations between the values obtained from the 18 distributions.

A number of additional studies have been performed to check the reliability of the $\alpha_s(M_Z^2)$ results obtained from experimentally optimized scales. In one of these studies 'optimized' renormalization scales as discussed in the literature are used to determine $\alpha_s(M_Z^2)$ in second order pertubation theory. The different methods applied for choosing an optimized scale lead to consistent results for the average value of $\alpha_s(M_Z^2)$. However, the scatter among $\alpha_s(M_Z^2)$ values from the individual distributions is smaller for the experimentally optimized scales than that obtained using theoretically motivated scale evaluation methods. The cor-

relation between the renormalization scales obtained with the different methods is also investigated.

Further determinations of $\alpha_s(M_Z^2)$ are performed by using all orders resummed calculations in the next-to-leading logarithmic approximation (NLLA). Here two different methods are applied. In the first case the pure NLLA predictions are confronted with the data in a limited fit range. In the second method α_s is determined using matched NLLA and $\mathcal{O}(\alpha_s^2)$ calculations. For both methods the renormalization scale is chosen to be $\mu = M_Z$. Both methods lead to average α_s values consistent with the average value obtained in $\mathcal{O}(\alpha_s^2)$ with experimentally optimized renormalization scales. The agreement between the results of the pure NLLA fits and those of the $\mathcal{O}(\alpha_s^2)$ is emphasized. A closer inspection of the fits in matched NLLA and $\mathcal{O}(\alpha_s^2)$ to the very precise data reveals a so far unreported problem with this method in that the trend of the data deviates systematically from the expectation of the matched theory.

The selection of hadronic events and the correction procedures applied to the data are described in Sect. 2. Section 3 introduces the investigated event shapes and compares the expectations from various fragmentation models. Section 4 contains the comparison with angular dependent second order QCD and a detailed discussion of the determination of $\alpha_s(M_Z^2)$. Section 5 summarises determinations of $\alpha_s(M_Z^2)$ using the renormalization scales discussed in the literature. Section 6 discusses results obtained by applying Padé approximants for the extrapolation of the pertubative predictions to higher orders. Section 7 discusses results from applying NLLA. The heavy quark mass correction of the $\alpha_s(M_Z^2)$ values derived from experimentally optimized renormalization scales is described in Sect. 8. The final results are summarized in the last section.

2 Detector and data analysis

In this analysis the final data measured with the DELPHI detector in 1994 at a centre-of-mass energy of $\sqrt{s} = M_Z$ are used. The statistics of the 1994 data is fully sufficient for the accurate QCD studies described in this paper. DELPHI is a hermetic detector with a solenoidal magnetic field of 1.2 T. The detector and its performance have been described in detail in [5]. The following components are relevant to this analysis:

- the Vertex Detector, VD, measuring charged particle track coordinates in the plane perpendicular to the beam with three layers of silicon micro-strip detectors at radii between 6.3 and 11 cm and covering polar angles, ϑ, with respect to the e^- beam between 37° and 143°;
- the Inner Detector, ID, a cylindrical jet chamber with a polar angle coverage from 17° to 163°;
- the Time Projection Chamber, TPC, the principal tracking detector of DELPHI, which has 6 sector plates in both the forward and backward hemispheres, each with 16 pad rows and 192 sense wires, inner and outer radii of 30 cm and 122 cm and covers polar angles from 20° to 160°;
- the Outer Detector, OD, a five layer drift chamber at 198 to 206 cm radius covering polar angles between 43° and 137°;
- two sets of forward planar drift chambers, FCA and FCB, with 6 and 12 layers respectively and overall polar angle coverages of 11° to 35° and 145° to 169°;
- the High Density Projection Chamber, HPC, a lead-glass electromagnetic calorimeter with a very good spatial resolution located inside the DELPHI coil between 208 cm and 260 cm radius and covering polar angles between 43° and 137°;
- the Forward Electromagnetic Calorimeter, FEMC, comprising two lead-glass arrays, one in each endcap, each consisting of 4500 lead-glass blocks with a projective geometry, and covering polar angles from 10° to 36.5° and from 143.5° to 170°;
- The hadron calorimeter, HAC, an iron-gas hadronic calorimeter outside the coil, consisting of 19 to 20 layers of streamer tubes and 5 cm thick iron plates also used as flux return, whose overall angular coverage is from 11.2° to 168.8°.

2.1 Event selection

Only charged particles in hadronic events were used. They were required to pass the following selection criteria:

- momentum, p, greater than 0.4 GeV/c,
- $\Delta p/p$ less than 100%,
- measured track length greater than 30 cm,
- track polar angle between 16° and 164°,
- impact parameter with respect to the nominal interaction point within 4 cm perpendicular to and 10 cm along the beam.

Hadronic events were selected by requiring:

- at least 5 charged particles,
- the total energy of charged particles greater than $12\%\sqrt{s}$ where the pion mass has been assumed for all particles,
- the charged energy in each hemisphere of the detector, defined by the plane perpendicular to the beam, E_{hemis}, greater than $3\%\sqrt{s}$,
- the polar angle of the thrust axis [1], ϑ_T, between 90.0° and 16.3°.

In total about 1.4 million events satisfy these cuts. The selection efficiency is 92%. Since the thrust axis does not distinguish between forward and backward directions, it is chosen such that $\cos\vartheta_T \geq 0$. ϑ_T is called the event orientation. The data are binned according to the event orientation into eight equal bins [2] of $\cos\vartheta_T$ between 0.0 and 0.96. With the exception of the eighth bin, the thrust axis is well contained within the detector acceptance.

[1] Thrust and the thrust axis have been calculated applying the algorithm included in the JETSET package [8].

[2] For the comparison of event shape observables with QCD predictions in all orders resummed next-to-leading-log approx-

2.2 Correction procedure

The contamination of beam gas events, $\gamma\gamma$ events and leptonic events other than $\tau^+\tau^-$, is expected to be less than 0.1 % and has been neglected. The influence of $\tau^+\tau^-$ events which have a pronounced 2-jet topology and contain high momentum particles has been determined by the KORALZ model [6] treated by the full simulation of the DELPHI detector DELSIM [7] and the standard data reconstruction chain. The $\tau^+\tau^-$ contributions have been subtracted from the measured data according to the relative rate of $\tau^+\tau^-$ $(0.46\% \pm 0.03\%)$ and hadronic events.

The observed data distributions were corrected for kinematic cuts, limited acceptance and resolution of the detector as well as effects due to reinteractions of particles inside the detector material. The simulated data were processed in the same way as the real data. The correction for initial state photon radiation has been determined using events generated by JETSET 7.3 PS [8] with and without initial state radiation as predicted by DYMU3 [9]. For any given observable Y the bin-by-bin correction factor $C(Y, \cos\vartheta_T)$ is calculated as:

$$C(Y,\cos\vartheta_T) = \frac{\left(\frac{1}{\sigma}\frac{d^2\sigma}{dY\,d\cos\vartheta_T}\right)^{DELSIM}_{generated}}{\left(\frac{1}{\sigma}\frac{d^2\sigma}{dY\,d\cos\vartheta_T}\right)^{DELSIM}_{reconstructed}} \cdot \frac{\left(\frac{1}{\sigma}\frac{d^2\sigma}{dY\,d\cos\vartheta_T}\right)^{noISR}}{\left(\frac{1}{\sigma}\frac{d^2\sigma}{dY\,d\cos\vartheta_T}\right)^{ISR}}. \quad (1)$$

Particles with a lifetime larger than 1 ns were considered as stable in the generated distributions. The bin widths were chosen on the basis of the estimated experimental resolution so as to minimize bin-to-bin migration effects.

For the evaluation of systematic errors the cuts for the track and event selections were varied over a wide range, including additional cuts on the momentum imbalance, etc. Variation of the tracking efficiency has been considered by discarding 2% of the accepted tracks at random. The influence of uncertainties in the momentum resolution was estimated by applying an additional Gaussian smearing of the inverse momenta of the simulated tracks. From the stability of the measured distributions a systematic uncertainty has been computed as the variance with respect to the central value. As the systematic error is expected to grow in proportion to the deviation of the overall correction factor from unity, an additional relative systematic uncertainty of 10% of this deviation has been added quadratically to the above value.

imation, the distributions have been integrated over ϑ_T. Differing from the event selection criteria listed above, the hadronic events were selected if the polar angle of the thrust axis satisfied $40.0^\circ < \vartheta_{\rm T} < 90.0^\circ$ for these angular integrated distributions.

3 Measured event shapes and comparison with fragmentation models

This analysis includes all commonly used shape observables which have a perturbative expansion known at least to next to leading order.

3.1 Definition of the observables

Thrust T is defined by [10] :

$$T = \max_{\vec{n}_T} \frac{\sum_i |\vec{p}_i \cdot \vec{n}_T|}{\sum_i |\vec{p}_i|}\,, \quad (2)$$

where $\vec{p}_i$ is the momentum vector of particle i, and $\vec{n}_T$ is the thrust axis to be determined.

Major M and Minor m are defined similarly, replacing $\vec{n}_T$ in the expression above by the Major axis $\vec{n}_{Maj}$, which maximizes the momentum sum transverse to $\vec{n}_T$ or the Minor axis $\vec{n}_{Min} = \vec{n}_{Maj} \times \vec{n}_T$ respectively.

The oblateness O is then defined by [11]:

$$O = M - m\,. \quad (3)$$

The C-parameter C is derived from the eigenvalues λ of the infrared-safe linear momentum tensor $\Theta^{i,j}$ [12]:

$$\Theta^{i,j} = \frac{1}{\sum_k |\vec{p}_k|} \cdot \sum_k \frac{p_k^i p_k^j}{|\vec{p}_k|} \quad (4)$$

$$C = 3 \cdot (\lambda_1\lambda_2 + \lambda_2\lambda_3 + \lambda_3\lambda_1)\,. \quad (5)$$

Here p_k^i denotes the i-component of $\vec{p}_k$.

Events can be divided into two hemispheres, a and b, by a plane perpendicular to the thrust axis $\vec{n}_T$. With M_a and M_b denoting the invariant masses of the two hemispheres, the normalized heavy jet mass $\rho_{\rm H}$, light jet mass $\rho_{\rm L}$, the sum of the jet masses $\rho_{\rm S}$ and their difference $\rho_{\rm D}$ can be defined as

$$\rho_H = \frac{\max(M_a^2, M_b^2)}{E_{vis}^2} \quad (6)$$

$$\rho_L = \frac{\min(M_a^2, M_b^2)}{E_{vis}^2} \quad (7)$$

$$\rho_S = \rho_H + \rho_L \quad (8)$$

$$\rho_D = \rho_H - \rho_L \quad (9)$$

where

$$E_{vis} = \sum_i E_i \quad (10)$$

and the energy of the particles i has been calculated assuming pion mass for charged and zero mass for neutral particles.

Jet broadening measures have been proposed in [13]. In both hemispheres a and b the transverse momenta of the particles are summed thus:

$$B_{a,b} = \frac{\sum_{i\in a,b} |\vec{p}_i \times \vec{n}_T|}{2\sum_i |\vec{p}_i|} . \tag{11}$$

The wide jet broadening $\mathrm{B_{max}}$, the narrow jet broadening $\mathrm{B_{min}}$, and the total jet broadening $\mathrm{B_{sum}}$ are then defined by

$$B_{max} = \max(B_a, B_b) \tag{12}$$

$$B_{min} = \min(B_a, B_b) \tag{13}$$

$$B_{sum} = B_{max} + B_{min} . \tag{14}$$

The first order prediction in perturbative QCD vanishes for both ρ_{L} and $\mathrm{B_{min}}$. Therefore these observables cannot be used for the determination of α_{s}.

Jet rates are commonly obtained using iterative clustering algorithms [14] in which a distance criterion or a metric y_{ij}, such as the scaled invariant mass, is computed for all pairs of particles i and j. The pair with the smallest y_{ij} is combined into a pseudoparticle (cluster) according to one of several recombination schemes. The clustering procedure is repeated until all of the y_{ij} are greater than a given threshold, the jet resolution parameter y_{cut}. The jet multiplicity of the event is defined as the number of clusters remaining; the n-jet rate $R_n(y_{cut})$ is the fraction of events classified as n-jet, and the differential two-jet rate is defined as

$$D_2(y_{cut}) = \frac{R_2(y_{cut}) - R_2(y_{cut} - \Delta y_{cut})}{\Delta y_{cut}} . \tag{15}$$

Several algorithms have been proposed differing from each other in their definition of y_{ij} and their recombination procedure. We apply the E0, P, P0, JADE [15], Durham [16], Geneva [14] and the Cambridge algorithms [17]. The definitions of the metrics y_{ij} and the recombination schemes for the different algorithms are given below.

In the E0 algorithm y_{ij} is defined as the square of the scaled invariant mass of the pair of particles i and j:

$$y_{ij} = \frac{(p_i + p_j)^2}{E_{vis}^2} . \tag{16}$$

The recombination is defined by:

$$E_k = E_i + E_j \ \ , \ \ \vec{p}_k = \frac{E_k}{|\vec{p}_i + \vec{p}_j|}(\vec{p}_i + \vec{p}_j) , \tag{17}$$

where E_i and E_j are the energies and $\vec{p}_i$ and $\vec{p}_j$ are the momenta of the particles.

In the P algorithm y_{ij} is defined by (16), and the recombination is defined by

$$\vec{p}_k = \vec{p}_i + \vec{p}_j \ \ , \ \ E_k = |\vec{p}_k| . \tag{18}$$

The P0 algorithm is defined similarly to the P algorithm, however the total energy E_{vis} (10) is recalculated at each iteration for the remaining pseudoparticles.

In the JADE algorithm, the definition of y_{ij} is

$$y_{ij} = \frac{2E_iE_j(1-\cos\theta_{ij})}{E_{vis}^2} , \tag{19}$$

where θ_{ij} is the angle between the pair of particles i and j.

For the Durham algorithm y_{ij} is given by

$$y_{ij} = \frac{2\min(E_i^2, E_j^2)(1-\cos\theta_{ij})}{E_{vis}^2} \tag{20}$$

and for the Geneva algorithm by

$$y_{ij} = \frac{8E_iE_j(1-\cos\theta_{ij})}{9(E_i+E_j)^2} . \tag{21}$$

For the algorithms given by (19), (20) and (21) the recombination is done by adding the particles four-momenta.

The recently proposed Cambridge algorithm [17] introduces an ordering of the particles i and j according to their opening angle, using the ordering variable

$$\nu_{ij} = 2(1-\cos\theta_{ij}) \tag{22}$$

and y_{ij} is defined by (20). The algorithm starts clustering from a table of N_{obj} primary objects, which are the particles' four-momenta, and proceeds as follows:

1. If only one object remains, store this as a jet and stop.
2. Select the pair of objects i and j that have the minimal value of the ordering variable ν_{ij} and calculate y_{ij} for that pair.
3. If $y_{ij} < y_{cut}$ then remove the objects i and j from the table and add the combined object with four-momentum $p_i + p_j$. If $y_{ij} \geq y_{cut}$ then store the object i or j with the smaller energy as a separated jet and remove it from the table. The higher energy object remains in the table.
4. go to 1.

The energy-energy correlation EEC [18] is defined in terms of the angle χ_{ij} between two particles i and j in an hadronic event:

$$EEC(\chi) = \frac{1}{N}\frac{1}{\Delta\chi}\sum_N\sum_{i,j}\frac{E_iE_j}{E_{vis}^2} \times \int_{\chi-\frac{\Delta\chi}{2}}^{\chi+\frac{\Delta\chi}{2}} \delta(\chi' - \chi_{ij})d\chi' , \tag{23}$$

where N is the total number of events, $\Delta\chi$ is the angular bin width and the angle χ is taken from $\chi = 0^\circ$ to $\chi = 180^\circ$.

The asymmetry of the energy-energy correlation AEEC is defined as

$$AEEC(\chi) = EEC(180^\circ - \chi) - EEC(\chi) . \tag{24}$$

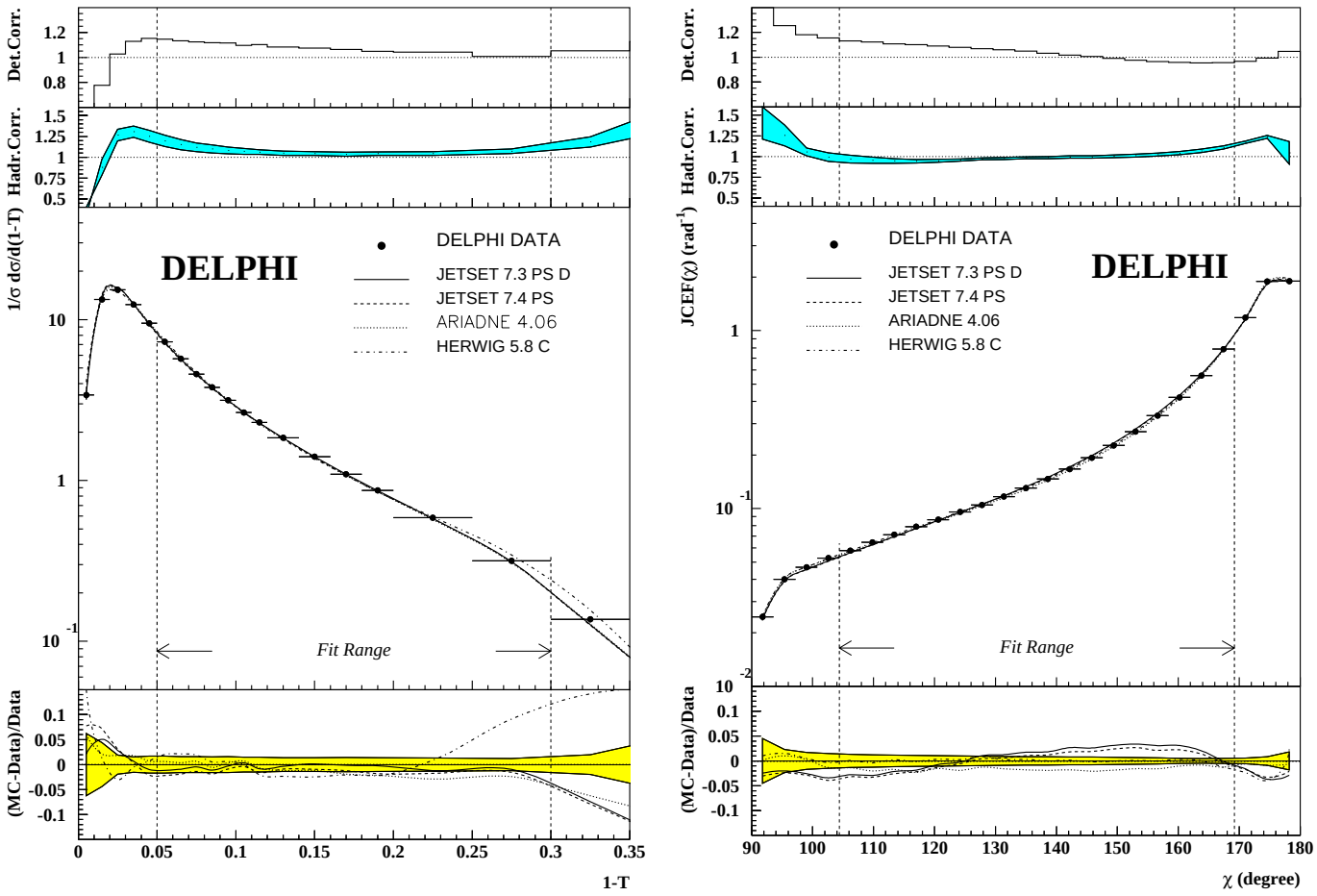

Fig. 1. *Left part:* Measured 1-T distribution integrated over $\cos\vartheta_{\mathrm{T}}$. The upper part shows the detector correction including effects due to initial state radiation. The part below shows the size of the hadronization correction. The width of the band indicates the uncertainty of the correction. In the central part the measured 1-T distribution is compared to the expectation from four hadronization generators, JETSET 7.3 PS D with DELPHI modification of heavy particle decays, JETSET 7.4 PS, ARIADNE 4.06 and HERWIG 5.8c. Also shown is the 1-T range used in the QCD fit. The lower part shows the ratio (Monte Carlo simulation-data)/data for the four hadronization generators. The width of the band indicates the size of the experimental errors. *Right part:* Same curves as shown in the left part but for JCEF integrated over $\cos\vartheta_{\mathrm{T}}$

The jet cone energy fraction JCEF [19] integrates the energy within a conical shell of an opening angle χ about the thrust axis. It is defined as

$$JCEF(\chi) = \frac{1}{N}\frac{1}{\Delta\chi}\sum_{N}\sum_{i}\frac{E_i}{E_{vis}} \times \int_{\chi-\frac{\Delta\chi}{2}}^{\chi+\frac{\Delta\chi}{2}} \delta(\chi'-\chi_i)d\chi' \,, \qquad (25)$$

where χ_i is the opening angle between a particle and the thrust axis vector $\vec{n}_T$, whose direction is defined here to point from the heavy jet mass hemisphere to the light jet mass hemisphere. Although the JCEF is a particularly simple and excellent observable for the determination of α_s , it has been rarely used until now in experimental measurements. Within an $\mathcal{O}(\alpha_s^2)$ analysis, the region $90^\circ < \chi \leq 180^\circ$, corresponding to the heavy jet mass hemisphere, can be used for the measurement of α_s . The distribution of the JCEF is shown in Fig. 1. Hadronization corrections and detector corrections as well as the next-to-leading order perturbative corrections are small. This allows a specially wide fit range to be used.

3.2 Fragmentation models

QCD based hadronization models, which describe well the distributions of the event shape observables in the hadronic final state of e^+e^- annihilation, are commonly used for modelling the transition from the primary quarks to the hadronic final state. Perturbative QCD can describe only a part of this transition, the radiation of hard gluons and the evolution of a parton shower. For a determination of the strong coupling constant α_s one has to take account of the so-called fragmentation or hadronization process, which is characterized by a small momentum transfer and hence a breakdown of perturbation theory. Several Monte Carlo models are in use to estimate

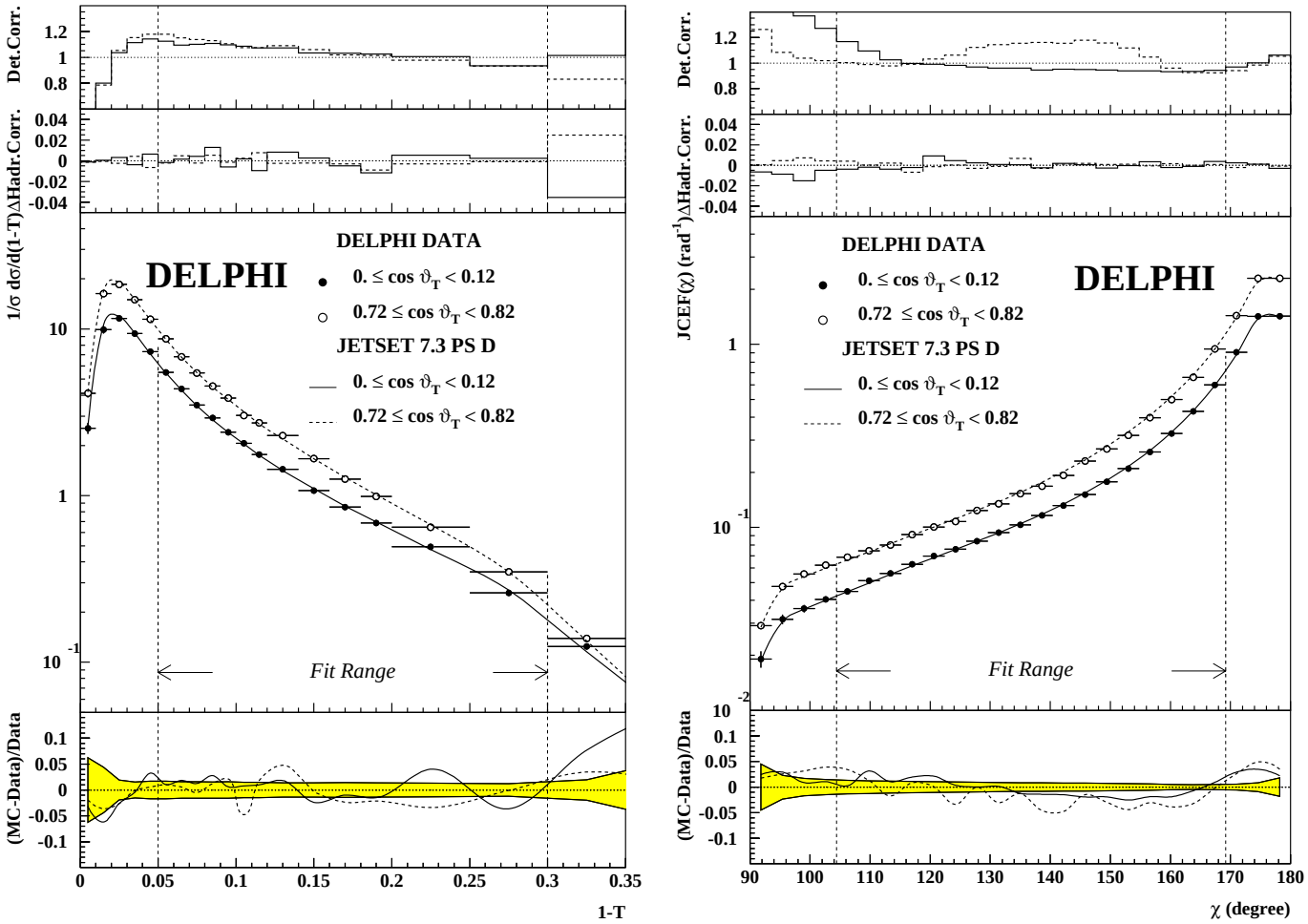

Fig. 2. *Left part:* Measured 1-T distribution in two bins of $\cos\vartheta_{\mathrm{T}}$. The upper part shows the detector corrections in the two $\cos\vartheta_{\mathrm{T}}$ bins. The part below shows the size of the relative hadronization correction in the two $\cos\vartheta_{\mathrm{T}}$ bins with respect to the average correction. In the central part the measured 1-T distributions are compared to JETSET 7.3 PS D. The lower part shows the ratio (Monte Carlo simulation-data)/data for the two $\cos\vartheta_{\mathrm{T}}$ bins. *Right part:* Same curves as shown in the left part but for JCEF in two bins of $\cos\vartheta_{\mathrm{T}}$

the size of the hadronization effects and the corresponding uncertainty. The most frequently used fragmentation models, namely JETSET 7.3 PS [8], ARIADNE 4.06 [20] and HERWIG 5.8c [21] have been extensively studied and tuned to DELPHI data and to identified particle spectra from all LEP experiments in [22]. As discussed in detail in [22] all models describe the data well. Examples of the measured hadron distributions are presented in Figs. 1 and 2. The increased systematic accuracy of the data is partially due to the fact that the ϑ_{T} dependence of the detector corrections is explicitly taken into account. The ϑ_T dependence of the detector corrections is shown, for instance, in Fig. 2 for two of the observables studied. Detailed tables of the individual event shape distributions including their statistical and systematic errors will be made available in the HEPDATA database [23]. For figures of the distributions see also [24].

Before theoretical expressions describing parton distributions can be compared with experimental data, corrections have to be made for hadronization effects, i.e. effects resulting from the transition of the parton state into the observed hadronic state. For the global event shape observables this transition is performed by a matrix P, where $\mathrm{P_{ij}}$ is the probability that an event contributing to the bin j of the partonic distribution will contribute to the bin i in the hadronic distribution and is computed from a Monte Carlo model. This probability matrix has been applied to the distributions from $\mathcal{O}(\alpha_s^2)$ perturbative theory $\mathrm{D_{pert.}}(\mathrm{Y},\cos\vartheta_{\mathrm{T}})$ to obtain the distributions for the predictions of the observed final state $\mathrm{D_{hadr.}}(\mathrm{Y},\cos\vartheta_{\mathrm{T}})$:

$$D_{hadr.}(Y,\cos\vartheta_T)_i = \sum_j P_{ij}(Y,\cos\vartheta_T) \times D_{pert.}(Y,\cos\vartheta_T)_j\,. \qquad (26)$$

In the case of the JCEF, EEC and AEEC, which are defined in terms of single particles and pairs of particles, respectively, bin-by-bin correction factors $\mathrm{C_{Hadr.}}$ similar to that described above for the detector effects have been computed such as:

$$D_{hadr.}(Y,\cos\vartheta_T)_i = C_{Hadr.}(Y,\cos\vartheta_T)_i$$

$$\times D_{pert.}(Y,\cos\vartheta_T)_i\,. \qquad (27)$$

Our reference model for evaluating hadronization effects is the JETSET 7.3 Parton Shower (PS) Generator, which has been modified with respect to the heavy particle decays to obtain a better description of the heavy particle branching fraction. This modified version is denoted by JETSET 7.3 PS D in the following. The tuned parameters have been taken from [22], where the updated tuning procedure is described in detail.

In order to estimate the systematic error of the hadronization correction, the analysis was repeated using alternative Monte Carlo generators with different hadronization models. In addition, the parameters for the JETSET PS were varied. A description of the models and their differences can be found for example in [22]. The alternative models used are ARIADNE 4.06, HERWIG 5.8c as well as version 7.4 JETSET PS [8]. All these models have been tuned to DELPHI data [22]. For our standard Monte Carlo program we applied also an alternative tuning to the DELPHI data which includes Bose-Einstein correlations, not included in the reference tuning. Whereas the number of hard gluons predicted by second order QCD matrix elements is simulated by the hadronization models [25], additional soft gluons are produced within the parton shower cascade, controlled by the JETSET PS parameter Q_0, which describes the parton virtuality at which the parton shower is stopped. To account for the sensitivity of the shape observables with respect to the additional soft gluons, Q_0 has been varied from 0.5 GeV to 4.0 GeV.

The systematic error of α_s originating from hadronization corrections is then estimated as the variance of the fitted α_s values obtained by using all the hadronization corrections mentioned above. Further studies have been made to investigate the influence of the main fragmentation parameters of the JETSET PS model by varying them within their experimental uncertainty. It has been found that this contribution to the uncertainty of α_s in general is less than one per mille, and has been neglected.

4 Comparison with angular dependent second order QCD using experimentally optimized scales

The evaluation of the $\mathcal{O}(\alpha_\mathrm{s}^2)$ coefficients is performed by using EVENT2 [26], a program for the integration of the $\mathcal{O}(\alpha_s^2)$ matrix elements. The algorithm is described in [1].

Using this program, one can calculate the double differential cross-section for any infrared and collinear safe observable Y in $\mathrm{e^+e^-}$ annihilation as a function of the event orientation:

$$\frac{1}{\sigma_{tot}}\frac{d^2\sigma(Y,\cos\vartheta_T)}{dY\,d\cos\vartheta_T} = \bar{\alpha}_s(\mu^2)\cdot A(Y,\cos\vartheta_T) + \bar{\alpha}_s^2(\mu^2) \cdot\left[B(Y,\cos\vartheta_T) + \Big(2\pi\beta_0\ln(x_\mu) - 2\Big)A(Y,\cos\vartheta_T)\right], \qquad (28)$$

where $\bar{\alpha}_\mathrm{s} = \alpha_\mathrm{s}/2\pi$ and $\beta_0 = (33-2n_f)/12\pi$, n_f is the number of active quark flavours and σ_{tot} is the one loop corrected cross-section for the process $\mathrm{e^+e^-} \to$ hadrons. The event orientation enters via ϑ_T, which denotes the polar angle of the thrust axis with respect to the $\mathrm{e^+e^-}$ beam direction. The renormalization scale factor x_μ is defined by $\mu^2 = x_\mu Q^2$ where $\mathrm{Q} = \mathrm{M_Z}$ is the centre-of-mass energy. A and B denote the $\mathcal{O}(\alpha_s)$ and $\mathcal{O}(\alpha_s^2)$ QCD coefficients, respectively. Alternatively, the double differential cross-section can be normalized to the partial cross-section in each $\cos\vartheta_\mathrm{T}$ interval:

$$R(Y,\cos\vartheta_T) = \left(\frac{d\sigma}{d\cos\vartheta_T}\right)^{-1}\frac{d^2\sigma(Y,\cos\vartheta_T)}{dY\,d\cos\vartheta_T} \qquad (29)$$

which is more appropriate for the study of residual QCD effects.

The strong coupling α_s at the renormalization scale μ is in second order perturbative QCD expressed as

$$\alpha_s(\mu) = \frac{1}{\beta_0\ln\frac{\mu^2}{\Lambda^2}}\left(1-\frac{\beta_1}{\beta_0^2}\frac{\ln\ln\frac{\mu^2}{\Lambda^2}}{\ln\frac{\mu^2}{\Lambda^2}}\right), \qquad (30)$$

where $\Lambda \equiv \Lambda^{(5)}_{\overline{\mathrm{MS}}}$ is the QCD scale parameter computed in the Modified Minimal Subtraction ($\overline{\mathrm{MS}}$) scheme for $n_f = 5$ flavours and $\beta_1 = (153-19n_f)/24\pi^2$.

The renormalization scale μ is a formally unphysical parameter and should not enter at all into an exact infinite order calculation [27]. Within the context of a truncated finite order perturbative expansion for any particular process under consideration, the definition of μ depends on the renormalization scheme employed, and its value is in principle completely arbitrary. This renormalization scale problem has been discussed extensively in the literature [4,27,28].

The traditional experimental approach to account for this problem has been to measure all observables at the same fixed scale value, the so-called physical scale $x_\mu = 1$ or equivalently $\mu^2 = \mathrm{Q}^2$. The scale dependence has been taken into account by varying μ over some wide ad hoc range, quoting the resulting change in the QCD predictions as theoretical uncertainty.

However, the approach of choosing $x_\mu = 1$ has a severe disadvantage. If we consider the ratio of the $\mathcal{O}(\alpha_s)$ and the $\mathcal{O}(\alpha_s^2)$ contributions to the cross-section, defined as

$$r_{NLO}(Y) = \frac{\alpha_s(x_\mu)\Big[B(Y)+A(Y)\big(2\pi\beta_0\ln(x_\mu)-2\big)\Big]}{A(Y)}, \qquad (31)$$

we find for many observables quite large values for the second order contributions. In some cases this ratio can have a magnitude approaching unity, indicating a poor convergence behavior of the $\mathcal{O}(\alpha_s^2)$ predictions in the $\overline{\mathrm{MS}}$ scheme which would quite naturally result in a wide spread of the measured α_s values. This has indeed been observed in previous analyses using $\mathcal{O}(\alpha_s^2)$ QCD [2,29,30].

Several proposals have been made which resolve the problem by choosing optimized scales according to different theoretical prescriptions [31–33]. These methods have

been discussed with some controversy [27] and until now no consensus has been achieved. The only approach for determining an optimized scale value, which does not rely on specific theoretical assumptions, is the experimental evaluation of an optimized $\mathcal{O}(\alpha_s^2)$ scale value x_μ for each measured observable separately. This strategy has therefore been chosen to be the primary method. For previous analyses including experimentally optimized renormalization scales see for example [29,34]. The theoretical approaches for choosing an optimized renormalization scale value are studied in detail in Sect. 5. As will be shown later, the approach of applying experimentally optimized scales yields an impressive consistency of the $\alpha_s(M_Z^2)$ measurements from different observables.

The procedure applied here, is a combined fit of α_s and the scale parameter x_μ. In the past this strategy suffered from a poor sensitivity of the fit with respect to x_μ for most of the observables. Due to the high statistics and high precision data now available, one may expect a better sensitivity at least for some of the observables under consideration.

We determined $\alpha_s(M_Z^2)$ and the renormalization scale factor x_μ simultaneously by comparing the corrected distributions for each observable Y with the perturbative QCD calculations corrected for hadronization effects as described in the previous section. The theoretical predictions have been fitted to the measured distributions $R(Y, \cos\vartheta_T)$ by minimizing χ^2, defined by using the sum of the squares of the statistical and systematic experimental errors, with respect to the variation of $\Lambda_{\overline{MS}}$ and x_μ.

The fit range for the central analysis, i.e. including the experimental optimization of x_μ, was chosen according to the following considerations:

- Requiring a detector acceptance larger than 80%, the last bin in $\cos\vartheta_{\mathrm{T}}$ was excluded in general, i.e. the fit range was restricted to the interval $0 \leq \cos\vartheta_{\mathrm{T}} < 0.84$ which corresponds to the polar angle interval $32.9^\circ < \vartheta_{\mathrm{T}} \leq 90.0^\circ$.
- Acceptance corrections were required to be below about 25% and the hadronization corrections to be below $\sim$ 40%.
- The contribution of the absolute value of the second order term $r_{NLO}(Y)$ as defined in (31) was required to be less than one[3] over the whole fit range.
- The requirement that the data can be well described by the theoretical prediction, i.e. χ^2/n_{df} is approximately 1 and stable over the fit range.
- Stability of the α_{s} - measurement with respect to the variation of the fit range.

For the analysis with a fixed renormalization scale value $x_\mu = 1$, the requirement that χ^2/n_{df} is approximately 1 can in general not be applied, since it would cause an unreasonably large reduction of the fit range for many observables. The thrust distribution for example could be fitted only over a range of at most three bins. For further details see also Sect. 4.2. The fit ranges for this analysis as well as for the analyses applying theoretically motivated scale setting methods have therefore been chosen identical to the analysis with experimentally optimized scale values, regardless of the χ^2 values of the fits.

[3] This requirement restricts the fit interval only for the total jet broadening observable B_{sum}, which yields rather large $\mathcal{O}(\alpha_s^2)$ contributions for any choice of the renormalization scale value.

4.1 Systematic and statistical uncertainties

For each observable the uncertainties from the fit of $\alpha_s(M_Z^2)$ and of x_μ have been determined by changing the parameters corresponding to a unit increase of χ^2. In the case of asymmetric errors the higher value was taken.

The systematic experimental uncertainty was estimated by repeating the analysis with different selections to calculate the acceptance corrections as described in Sect. 2. Additionally, an analysis was performed including neutral clusters measured with the hadronic and/or electromagnetic calorimeters. The overall uncertainty was taken as the variance of the individual $\alpha_s(M_Z^2)$ measurements.

An additional source of experimental uncertainty arises from the determination of the fit range, which has been estimated by varying the lower and the upper edge of the fit range by ± 1 bin, respectively, while the other edge is kept fixed. Half of the maximum deviation in $\alpha_s(M_Z^2)$ has been taken as the error due to the variation of the fit range and has been added in quadrature.

The hadronization uncertainty was determined as described in Sect. 3.

The total uncertainty on $\alpha_s(M_Z^2)$ is determined from the sum of the squares of the errors listed above.

Uncertainties due to missing higher order calculations

An additional source of theoretical uncertainty arises due to the missing higher order calculations of perturbative QCD. It is commonly assumed, that the size of these uncertainties can be estimated by varying the renormalization scale value applied for the determination of $\alpha_s(M_Z^2)$ within some 'reasonable' range [35]. The choice of a 'reasonable' range involves subjective jugdement and so far no common agreement about the size of this range has been achieved. Furthermore, this commonly used approach has been criticized in the literature [4]. According to [4] any artificial increase of the uncertainty of $\alpha_s(M_Z^2)$ due to a large variation of the renormalization scale should be avoided so that the degree of precision to which QCD can be tested remains transparent. It should be pointed out that no such additional uncertainty is required to understand the scatter of the measurements from a large number of observables if experimentally optimized renormalization scale values are applied. This will be demonstrated in the following section. Other procedures for estimating uncertainties due to missing higher order corrections have been suggested, in particular the comparison of $\alpha_s(M_Z^2)$ values obtained by applying different reasonable renormalization schemes or by replacing the missing higher order terms by

Table 1. Observables used in the $\mathcal{O}(\alpha_s^2)$ QCD fits. For each of the observables the fit range, the range in $\cos\vartheta_T$, the measured renormalization scale factor x_μ together with the uncertainty as determined from the fit, the χ^2/n_{df} and the number of degrees of freedom n_{df} are shown. In the case of asymmetric errors the higher value is given

Observable	Fit Range	$\cos\vartheta_T$ Range	x_μ	χ^2/n_{df}	n_{df}
EEC	$28.8^\circ - 151.2^\circ$	0.0 - 0.84	0.0112 ± 0.0006	1.02	236
AEEC	$25.2^\circ - 64.8^\circ$	0.0 - 0.84	0.0066 ± 0.0018	0.98	75
JCEF	$104.4^\circ - 169.2^\circ$	0.0 - 0.84	0.0820 ± 0.0046	1.05	124
$1-\mathrm{T}$	0.05 - 0.30	0.0 - 0.84	0.0033 ± 0.0002	1.24	89
O	0.24 - 0.44	0.0 - 0.84	2.30 ± 0.40	0.90	33
C	0.24 - 0.72	0.0 - 0.84	0.0068 ± 0.0006	1.02	82
$\mathrm{B_{Max}}$	0.10 - 0.24	0.0 - 0.84	0.0204 ± 0.0090	0.89	47
$\mathrm{B_{Sum}}$	0.12 - 0.24	0.0 - 0.84	0.0092 ± 0.0022	1.19	40
ρ_H	0.03 - 0.14	0.0 - 0.84	0.0036 ± 0.0004	0.63	54
ρ_S	0.10 - 0.30	0.0 - 0.36	0.0027 ± 0.0019	0.82	16
ρ_D	0.05 - 0.30	0.0 - 0.84	2.21 ± 0.38	1.02	68
$\mathrm{D_2^{E0}}$	0.07 - 0.25	0.0 - 0.84	0.048 ± 0.020	0.85	68
$\mathrm{D_2^{P0}}$	0.05 - 0.18	0.0 - 0.84	0.112 ± 0.048	1.02	68
$\mathrm{D_2^{P}}$	0.10 - 0.25	0.0 - 0.84	0.0044 ± 0.0004	1.00	47
$\mathrm{D_2^{Jade}}$	0.06 - 0.25	0.0 - 0.84	0.126 ± 0.049	1.05	75
$\mathrm{D_2^{Durham}}$	0.015 - 0.16	0.0 - 0.84	0.0126 ± 0.0015	0.92	96
$\mathrm{D_2^{Geneva}}$	0.015 - 0.03	0.0 - 0.84	7.10 ± 0.28	0.84	19
$\mathrm{D_2^{Cambridge}}$	0.011 - 0.18	0.0 - 0.84	0.066 ± 0.019	0.98	145

Table 2. Individual sources of errors of the $\alpha_s(M_\mathrm{Z}^2)$ measurement. For each observable, the value of $\alpha_s(M_\mathrm{Z}^2)$, the experimental uncertainty (statistical and systematic), the uncertainty resulting from hadronization corrections, the theoretical uncertainty due to scale variation around the central value x_μ^{exp} in the range $0.5{\cdot}x_\mu^{exp} \le x_\mu \le 2{\cdot}x_\mu^{exp}$ and the total uncertainty are shown

Observable	$\alpha_s(M_\mathrm{Z}^2)$	$\Delta\alpha_s$ (Exp.)	$\Delta\alpha_s$ (Hadr.)	$\Delta\alpha_s$ (Scale.)	$\Delta\alpha_s$ (Tot.)
EEC	0.1142	$\pm$ 0.0007	$\pm$ 0.0023	$\pm$ 0.0014	$\pm$ 0.0028
AEEC	0.1150	$\pm$ 0.0037	$\pm$ 0.0029	$\pm$ 0.0100	$\pm$ 0.0111
JCEF	0.1169	$\pm$ 0.0006	$\pm$ 0.0013	$\pm$ 0.0008	$\pm$ 0.0017
$1-\mathrm{T}$	0.1132	$\pm$ 0.0009	$\pm$ 0.0026	$\pm$ 0.0023	$\pm$ 0.0036
O	0.1171	$\pm$ 0.0028	$\pm$ 0.0030	$\pm$ 0.0038	$\pm$ 0.0056
C	0.1153	$\pm$ 0.0021	$\pm$ 0.0023	$\pm$ 0.0017	$\pm$ 0.0036
$\mathrm{B_{Max}}$	0.1215	$\pm$ 0.0022	$\pm$ 0.0031	$\pm$ 0.0013	$\pm$ 0.0041
$\mathrm{B_{Sum}}$	0.1138	$\pm$ 0.0030	$\pm$ 0.0032	$\pm$ 0.0030	$\pm$ 0.0053
ρ_H	0.1215	$\pm$ 0.0014	$\pm$ 0.0029	$\pm$ 0.0050	$\pm$ 0.0060
ρ_S	0.1161	$\pm$ 0.0014	$\pm$ 0.0018	$\pm$ 0.0016	$\pm$ 0.0033
ρ_D	0.1172	$\pm$ 0.0013	$\pm$ 0.0034	$\pm$ 0.0007	$\pm$ 0.0038
$\mathrm{D_2^{E0}}$	0.1165	$\pm$ 0.0027	$\pm$ 0.0029	$\pm$ 0.0017	$\pm$ 0.0044
$\mathrm{D_2^{P0}}$	0.1210	$\pm$ 0.0018	$\pm$ 0.0026	$\pm$ 0.0009	$\pm$ 0.0033
$\mathrm{D_2^{P}}$	0.1187	$\pm$ 0.0019	$\pm$ 0.0021	$\pm$ 0.0036	$\pm$ 0.0046
$\mathrm{D_2^{Jade}}$	0.1169	$\pm$ 0.0011	$\pm$ 0.0020	$\pm$ 0.0028	$\pm$ 0.0040
$\mathrm{D_2^{Durham}}$	0.1169	$\pm$ 0.0013	$\pm$ 0.0016	$\pm$ 0.0015	$\pm$ 0.0026
$\mathrm{D_2^{Geneva}}$	0.1178	$\pm$ 0.0052	$\pm$ 0.0075	$\pm$ 0.0295	$\pm$ 0.0309
$\mathrm{D_2^{Cambridge}}$	0.1164	$\pm$ 0.0008	$\pm$ 0.0023	$\pm$ 0.0004	$\pm$ 0.0025

Table 3. Results of the $\alpha_s(M_Z^2)$ measurements using a fixed renormalization scale $x_\mu = 1$. For each observable, the value of $\alpha_s(M_Z^2)$, the uncertainty from the variation of the scale between $0.5 \leq x_\mu \leq 2$, the total uncertainty and the χ^2/n_{df} of the fit are shown

Observable	$\alpha_s(M_Z^2)$	$\Delta\alpha_s$ (Scale)	$\Delta\alpha_s$ (Tot.)	χ^2/n_{df}
EEC	0.1297	$\pm$ 0.0037	$\pm$ 0.0042	10.7
AEEC	0.1088	$\pm$ 0.0015	$\pm$ 0.0050	2.04
JCEF	0.1191	$\pm$ 0.0012	$\pm$ 0.0024	7.7
$1-T$	0.1334	$\pm$ 0.0042	$\pm$ 0.0051	25.9
O	0.1211	$\pm$ 0.0065	$\pm$ 0.0077	2.38
C	0.1352	$\pm$ 0.0043	$\pm$ 0.0053	12.0
B_{Max}	0.1311	$\pm$ 0.0073	$\pm$ 0.0083	1.67
B_{Sum}	0.1403	$\pm$ 0.0056	$\pm$ 0.0071	8.1
ρ_H	0.1325	$\pm$ 0.0036	$\pm$ 0.0049	5.1
ρ_S	0.1441	$\pm$ 0.0055	$\pm$ 0.0062	2.16
ρ_D	0.1181	$\pm$ 0.0012	$\pm$ 0.0039	1.54
D_2^{E0}	0.1267	$\pm$ 0.0033	$\pm$ 0.0052	1.35
D_2^{P0}	0.1265	$\pm$ 0.0026	$\pm$ 0.0041	1.31
D_2^{P}	0.1154	$\pm$ 0.0019	$\pm$ 0.0036	5.35
D_2^{Jade}	0.1249	$\pm$ 0.0030	$\pm$ 0.0042	1.53
D_2^{Durham}	0.1222	$\pm$ 0.0034	$\pm$ 0.0046	3.47
D_2^{Geneva}	0.0735	$\pm$ 0.0071	$\pm$ 0.0116	120.
$D_2^{Cambridge}$	0.1202	$\pm$ 0.0021	$\pm$ 0.0033	1.32

their Padé Approximants [35]. Both strategies have been studied. By comparing the size of the uncertainties derived applying these methods (see e.g. Table 11), a variation of x_μ between $0.5{\cdot}x_\mu^{exp}$ and $2{\cdot}x_\mu^{exp}$ seems justified to obtain an estimate of these uncertainties. Similar or identical ranges have for example also been chosen in [3,56].

4.2 Results

The results of the fits to the 18 event shape distributions are summarized in tables 1 and 2 and shown in Fig. 3. It should be noted that for all observables the normalized χ^2 is about one for a typically large number of degrees of freedom ($n_{df} = 16 - 236$, see Table 1). The individual errors contributing to the total error on the value of α_s are listed in Table 2. Among the observables considered the JCEF yields the most precise result.

For comparison, the data have also been fitted in $\mathcal{O}(\alpha_s^2)$ applying a fixed renormalization scale value $x_\mu = 1$. The results of these fits are summarized in Table 3 and shown in Fig. 4. As can be seen from the χ^2/n_{df} values of the fits, the choice of $x_\mu = 1$ yields only a poor description of the data for most of the observables, for many observables the description is even unacceptable.

More details concerning the QCD fits are presented in Figs. 5 to 9. Figure 5 shows the values of $\alpha_s(M_Z^2)$ and the corresponding values of $\Delta\chi^2$, i.e. the change of χ^2 with respect to the optimal value, for the fits as a function of the scale $\lg(x_\mu)$ for some of the investigated observables.

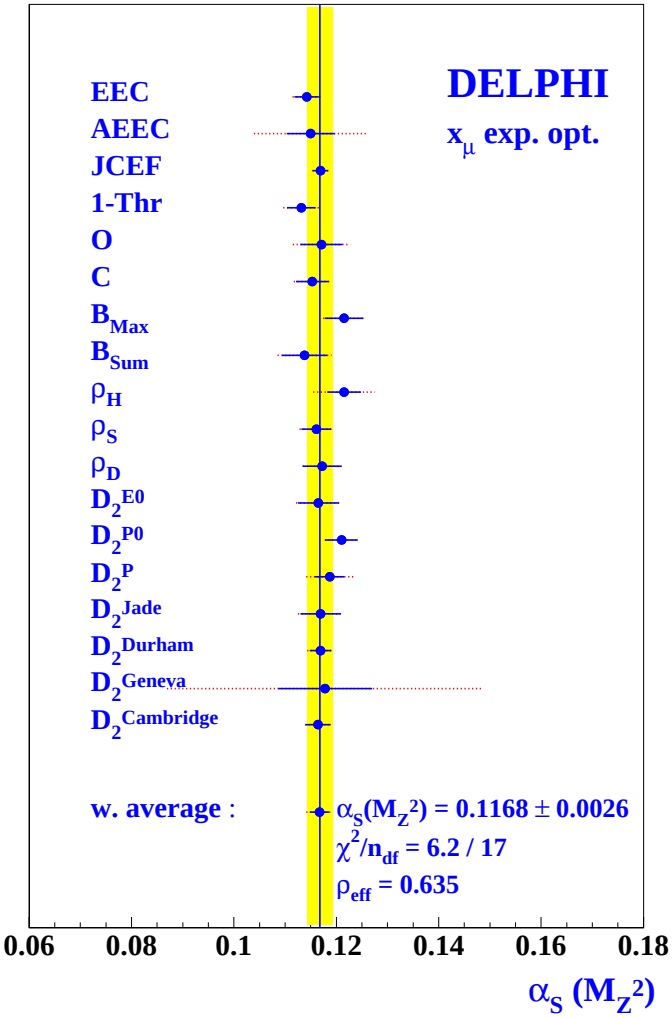

Fig. 3. Results of the QCD fits applying experimentally optimized scales for 18 event shape distributions. The error bars indicated by the solid lines are the quadratic sum of the experimental and the hadronization uncertainty. The error bars indicated by the dotted lines include also the additional uncertainty due to the variation of the renormalization scale due to scale variation around the central value x_μ^{exp} in the range $0.5 \cdot x_\mu^{exp} \leq x_\mu \leq 2 \cdot x_\mu^{exp}$. Also shown is the correlated weighted average (see text). The χ^2-value is given before readjusting according to 33

The shape of the $\Delta\chi^2$ curves indicates that for most distributions the renormalization scale has to be fixed to a rather narrow range of values in order to be consistent with the data. For most of the observables the renormalization scale dependence of $\alpha_s(M_Z^2)$ is significantly smaller in the region of the scale value for the minimum in χ^2/n_{df} than for the region around $x_\mu = 1$. It should however be noted, that even for observables exhibiting a strong scale dependence of $\alpha_s(M_Z^2)$, e.g. D_2^{Geneva}, the $\alpha_s(M_Z^2)$ value for the experimentally optimized scale value is perfectly consistent with the average value.

Figures 6 to 9 contain a direct comparison of the data measured at various bins in $\cos\vartheta_T$ with the results of the

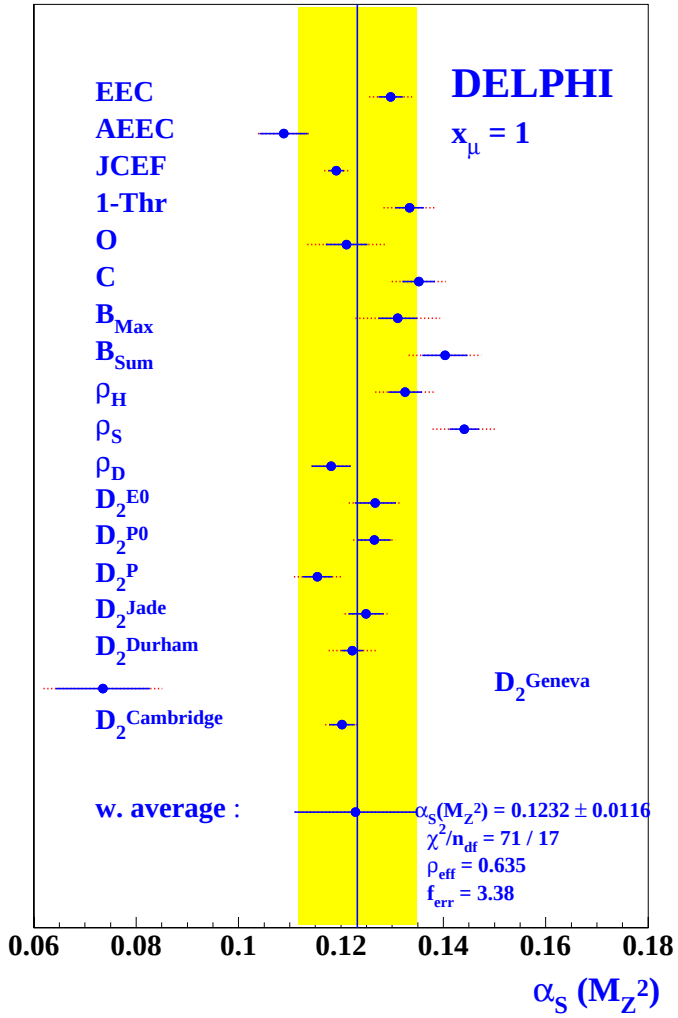

Fig. 4. Results of the QCD fits applying a fixed renormalization scale $x_\mu = 1$. The error bars indicated by the solid lines are the quadratic sum of the experimental and the hadronization uncertainty. The error bars indicated by the dotted lines include also the additional uncertainty due to the variation of the renormalization scale around the central value x_μ^{exp} from $0.5 \cdot x_\mu^{exp} \leq x_\mu \leq 2 \cdot x_\mu^{exp}$. Also shown is the correlated weighted average. It has been calculated assuming the same effective correlation $\rho_{\rm eff} = 0.635$ as for the fit results applying experimentally optimized scales. The χ^2/n_{df} for the weighted average is 71/17, where the χ^2 given corresponds to the value before adjusting $\rho_{\rm eff}$. In order to yield $\chi^2/n_{df} = 1$, the errors have to be scaled by a factor $f_{\rm err} = 3.38$

QCD fits. The measured dependence on both $\cos\vartheta_{\rm T}$ and the studied observable are precisely reproduced by the fits.

At this point a comparison with the results from applying a fixed renormalization scale value $x_\mu = 1$ seems appropriate. Figure 10 shows QCD fits to the data with experimentally optimized and with fixed renormalization scale values $x_\mu = 1$ for the observables $1-T$, ρ_H and D_2^P. It can be seen that the slope of the experimental distributions cannot be described by the theoretical prediction applying $x_\mu = 1$. The same observation has also been made for other observables. Good description of the data can in general only be achieved within the small kinematical region where the fit curve intersects with the data. Demanding $\chi^2/n_{df} \backsimeq 1$ the thrust distribution for example can only be described within a maximum range of three bins in 1-T. It should be noted, that in contrast to fits applying experimentally optimized scales, the stability of $\alpha_s(M_{\rm Z}^2)$ with respect to the choice of the fit range is in general quite poor. This observation is new and due to the fact that the data used in this analysis have both smaller statistical and systematical errors than in previous publications. (See also Sect. 4.3).

Combining the 18 individual results from the $\alpha_s(M_{\rm Z}^2)$ measurements applying experimentally optimized renormalization scale values by using an unweighted average yields

$$\alpha_s(M_{\rm Z}^2) \ = 0.1170 \pm 0.0025$$

whereas the corresponding average for the measurements using the fixed scales $x_\mu = 1$ is $\alpha_s(M_{\rm Z}^2) = 0.1234 \pm 0.0154$. For the experimentally optimized scales the scatter of the individual measurements is significantly reduced.

The consistency of the individual measurements using experimentally optimized scales is clearly shown by the good $\chi^2/n_{df} = 9.6/17$ for the unweighted average. This value is computed on the basis of the total uncertainty (experimental and hadronization uncertainty) without considering an additional renormalization scale error. For the average of the fixed scale $x_\mu = 1$ measurements $\chi^2/n_{df} = 168/17$, thus in this case the individual measurements are clearly inconsistent with each other. This inconsistency may be understood to arise from the imperfect description of the data for the fits with $x_\mu = 1$, which cause α_s , the parameter of the fit, not to be well defined.

The idea behind the common analysis of such a large number of observables is to optimize the use of the information contained in the complex structure of multihadron events. Errors due to the corrections for hadronization effects may be expected to cancel to some extent in the averaging procedure. To test this expectation the analysis of each of the individual 18 observables is repeated by performing hadronization corrections with all hadronization generators described in Sect. 3.2. This results in 7 times 18 individual $\alpha_{\rm s}$ values. As a first test for each of the 18 observables the unweighted average value of $\alpha_{\rm s}$ from the seven models is evaluated. The average value of the 18 $\alpha_{\rm s}$ values is $\alpha_s(M_{\rm Z}^2) = 0.1177 \pm 0.0029$. In a second step for each of the 7 hadronization models an unweighted average of the corresponding 18 $\alpha_{\rm s}$ values is calculated. Finally an unweighted average of the 7 average values for the different hadronization models is computed resulting in $\alpha_s(M_{\rm Z}^2) = 0.1177 \pm 0.0016$. The result confirms that the scatter of the average values due to different assumptions for hadronization corrections is significantly smaller than the uncertainty of ± 0.0025 of the mean value from 18 individual observables.

The correlations between the α_s values obtained from the different observables must be taken into account in order to calculate their weighted average. Since the correlations are mostly unknown, the exact correlation pattern

cannot be worked out reliably. Therefore, we use a recently proposed method [36], which makes use of a robust estimation of the covariance matrix and has been used for example in [37]. Here it is assumed that different measurements i and j are correlated with a fixed fraction $\rho_{\rm eff}$ of the maximum possible correlation $\mathrm{C_{ij}^{max}}$:

$$C_{ij} = \rho_{\rm eff} C_{ij}^{max} \quad i \neq j, \quad \text{with} \quad C_{ij}^{max} = \sigma_i \sigma_j \,. \quad (32)$$

For $\rho_{\rm eff} = 0$ the measurements are treated as uncorrelated, for $\rho_{\rm eff} = 1$ as 100% correlated entities. When $\chi^2 < n_{df}$ the measurements are assumed to be correlated and the value $\rho_{\rm eff}$ then is adjusted such that the χ^2 is equal to the number of degrees of freedom n_{df}:

$$\begin{aligned}\chi^2(\rho_{\rm eff}) &= \sum_{i,j}(x_i - \overline{x})(x_j - \overline{x})(C^{-1})_{ij} \\ &= n - 1 = n_{df} \,. \end{aligned} \quad (33)$$

When $\chi^2 > n_{df}$ it is assumed that the errors of the measurement are underestimated and will therefore be scaled until $\chi^2 = n_{df}$ is satisfied.

Applying this method to the 18 observables studied, the weighted average (see also Fig. 3) yields:

$$\alpha_s(M_{\rm Z}^2) \ = 0.1168 \pm 0.0026$$

with $\rho_{\rm eff}$ being 0.635. Both the central value and its uncertainty are almost identical to the unweighted average and the r.m.s. quoted above, which in itself is a remarkable result.

It should be noted, that the method applied for the calculation of the weighted average does not necessarily lead to the smallest possible error. In [37] it is shown for example, that the error of the weighted average is increased if less significant measurements are included. Within this analysis however, the α_s measurements from all individual observables have been considered, regardless of their significance. This is motivated by the fact that the errors of the α_s measurements quoted in Table 2 and in the following subsections contain all uncertainties which can be evaluated from a careful experimental analysis. However, the spread of the α_s measurements may not be explainable by the individual uncertainties alone, there may be additional uncertainties, which cannot be derived from a single observable. Therefore the above averaging procedure has been applied and robustness of the error estimate has been preferred instead of minimizing the error. Still this error estimate may not cover a possible general shift of the measured average with respect to the true $\alpha_s(M_{\rm Z}^2)$ value. Apart from a better theoretical understanding, today such a shift could only be inferred by comparing to different types of calculation, like resummed or Padé approximation, which are presented in Sects. 6 and 7.

4.3 Additional cross checks

An underlying assumption for the $\mathcal{O}(\alpha_s^2)$ QCD fits to the shape observables is that the value of α_s is approximately independent of a variation of the renormalization scale within the fit range. To check this assumption, a cross check for the differential two jet rate observables has been performed following a suggestion in [38]. For these observables the QCD fits have been repeated, allowing the renormalization scale to vary proportionally to y_{cut}, i.e. $\mu^2 = x_\mu y_{cut} \sqrt{s}$. The differences in the $\alpha_s(M_{\rm Z}^2)$ determination have been found to be of the order of a few per mille for the individual jet rate observables and to be less than two per mille for the average of these observables.

A further investigation has been performed for all observables of Table 1. The fit range listed in Table 1 has been divided into two separate, approximately symmetrical regions, allowing a maximum overlap of one bin. $\alpha_s(M_{\rm Z}^2)$ has been determined applying experimentally optimized scales for both regions independently. The fits were successful for all observables except D_2^{Geneva}, where the resulting fit ranges were too small to allow the fits to converge. Good agreement of the two α_s values measured for each observable is found. In a further step, the two $\alpha_s(M_{\rm Z}^2)$ values have been combined for each observable according to their statistical weight. These α_s values have been combined by calculating a weighted average as described before. The resulting average value of $\alpha_s(M_Z^2) = 0.1168 \pm 0.0025$ is identical to the value determined from the standard procedure. No systematical trend of the two values of the renormalization scales found for the two fit ranges (dominated by two respectively three jet events) is observed.

5 Scale setting methods from theory

Several methods for the choice of an optimized value for the renormalization scale have been suggested by theory. See e.g. [28] for an overview. In this section we compare the $\alpha_s(M_Z^2)$ measurements, using renormalization scales predicted by three different approaches with the $\alpha_s(M_Z^2)$ measurements using experimentally optimized scales:

(*i*) The principle of minimal sensitivity (PMS). Since all order predictions should be independent of the renormalization scale, Stevenson [31] suggests choosing the scale to be least sensitive with respect to its variation, i.e. from the solution of

$$\frac{\partial \sigma}{\partial x_\mu} = 0 \ . \quad (34)$$

(*ii*) The method of effective charges (ECH). The basic idea of this approach [32] is to choose the renormalization scheme in such a way that the relation between the physical quantity and the coupling is the simplest possible one. In $\mathcal{O}(\alpha_s^2)$, where the ECH approach is equivalent to the method of fastest apparent convergence (FAC) [32] the scale is chosen in such a way that the second order term in (28) vanishes:

$$B(Y, \cos\vartheta_T) + \big(2\pi\beta_0 \ln(x_\mu) - 2\big) A(Y, \cos\vartheta_T) = 0. \quad (35)$$

(*iii*) The method of Brodsky, Lepage and MacKenzie (BLM) [33]. This method follows basic ideas in QED,

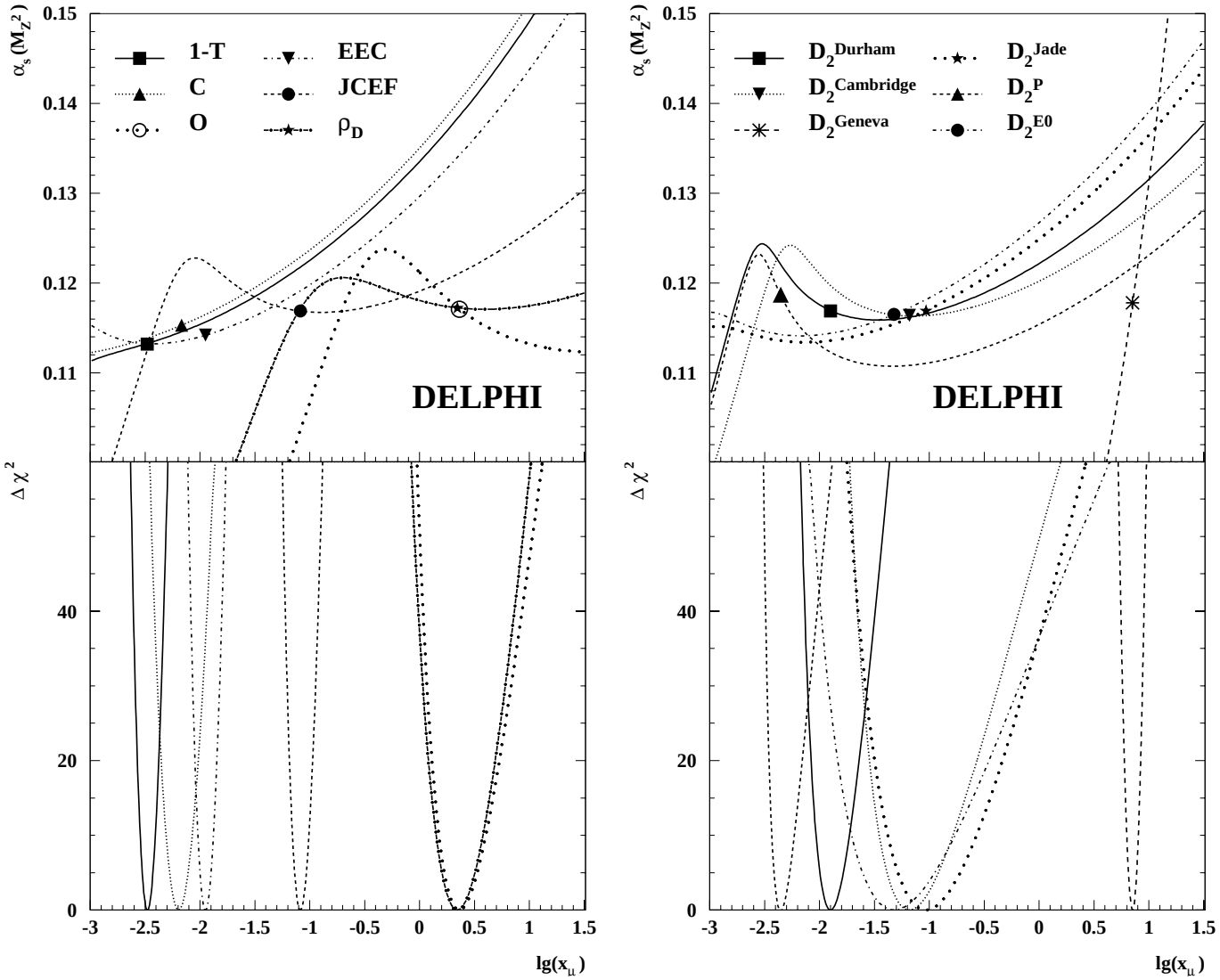

Fig. 5. (*Left side*) $\alpha_s(M_Z^2)$ and $\Delta\chi^2 = \chi^2 - \chi^2_{\rm min}$ from $\mathcal{O}(\alpha_s^2)$ fits to the double differential distributions in $\cos\vartheta_{\rm T}$ and $1-{\rm T}$, C, O, EEC, JCEF, ρ_D . Additionally, the χ^2 minima are indicated in the $\alpha_s(M_Z^2)$ curves. (*Right side*) The same for the double differential distributions in $\cos\vartheta_{\rm T}$ and the differential 2-jet rate applying the Durham, Cambridge, Geneva, Jade, P and E0 jet algorithm

where the renormalized electric charge is fully given by the vacuum polarization due to charged fermion-antifermion pairs [28]. In QCD it is suggested to fix the scale with the requirement that all the effects of quark pairs be absorbed in the definition of the renormalized coupling itself. In $\mathcal{O}(\alpha_s^2)$ this amounts to the requirement that x_μ is chosen in such a way that the flavour dependence n_f of the second order term in Eq. 28 is removed:

$$\frac{\partial}{\partial n_f}\left\{B(Y,n_f) + \big(2\pi\beta_0\ln(x_\mu) - 2\big)A(Y)\right\}\Bigg|_{n_f=5} = 0. \quad (36)$$

The results of the $\alpha_s(M_Z^2)$ measurements for the individual observables applying the different scale setting prescriptions are listed in Table 4. The weighted averages for the different methods yield:

(*i*) PMS method :

$\alpha_{\rm s}({\rm M_Z^2}) = 0.1154 \pm 0.0045 \qquad (\chi^2/{\rm n_{df}} = 19/17)$

(*ii*) ECH method :

$\alpha_{\rm s}({\rm M_Z^2}) = 0.1155 \pm 0.0044 \qquad (\chi^2/{\rm n_{df}} = 19/17)$

(*iii*) BLM method :

$\alpha_{\rm s}({\rm M_Z^2}) = 0.1174 \pm 0.0068 \qquad (\chi^2/{\rm n_{df}} = 29/13)$

to be compared with $\alpha_{\rm s}({\rm M_Z^2}) = 0.1168 \pm 0.0026$ ($\chi^2/n_{df} = 6.2/17$) using the experimentally optimized scales.

The weighted averages for the different theoretical methods are in agreement with the average using experimentally optimized scales. The scatter of the individual measurements is lowest for the experimentally optimized

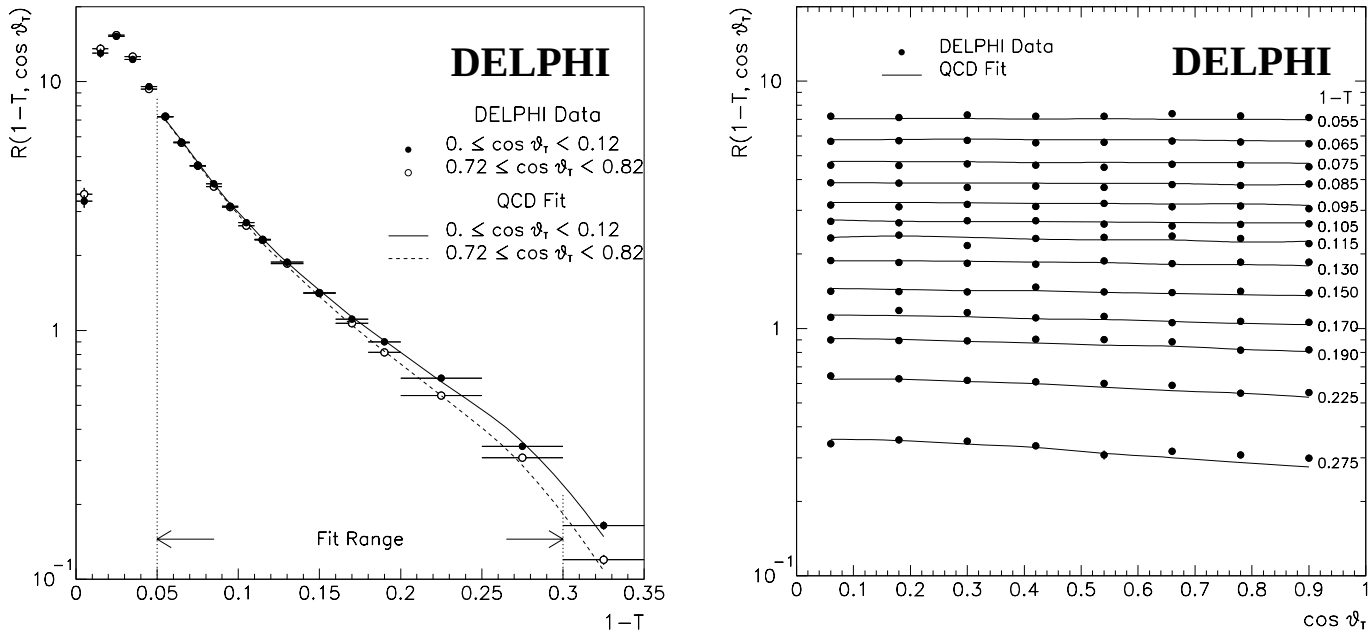

Fig. 6. (*Left side*) QCD fits to the measured thrust distribution for two bins in $\cos\vartheta_{\mathrm{T}}$. (*Right side*) Measured thrust distribution at various fixed values of $1-\mathrm{T}$ as a function of $\cos\vartheta_{\mathrm{T}}$. The solid lines represent the QCD fit

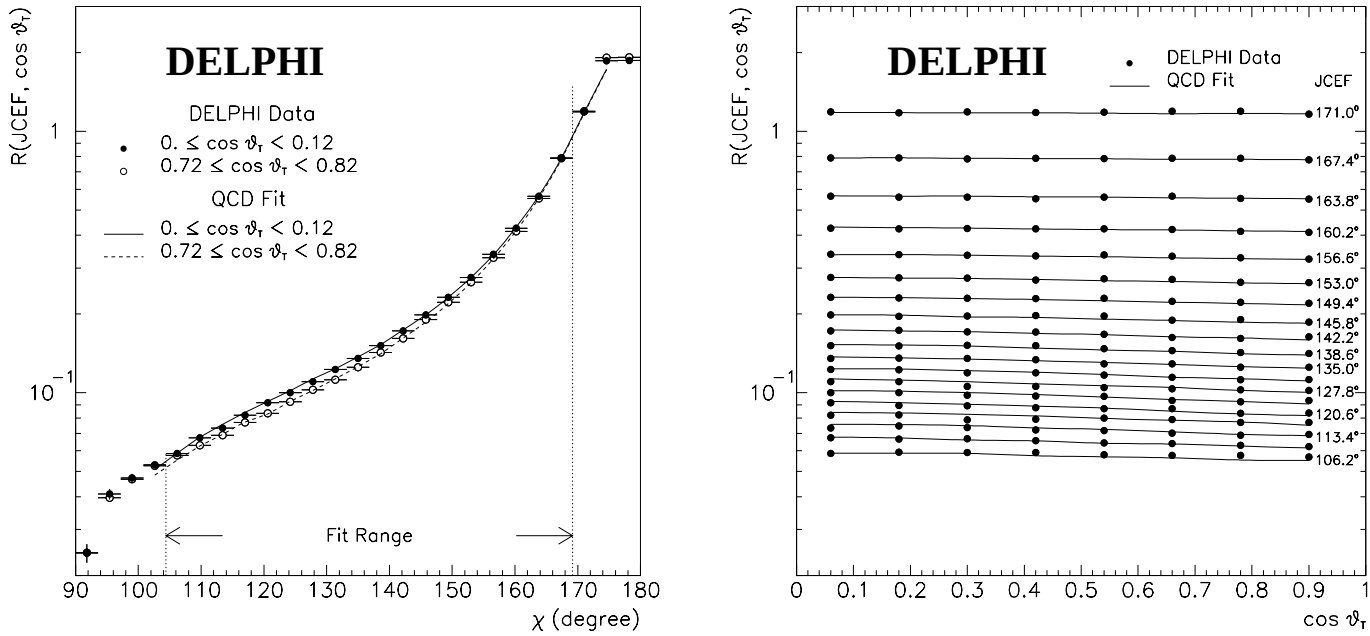

Fig. 7. Same as Fig. 6 but for the jet cone energy fraction JCEF

scales and highest for the BLM method. Whereas for the experimentally optimized scales the fit values for the individual $\alpha_s(M_{\mathrm{Z}}^2)$ measurements are perfectly consistent, the consistency for the ECH and the PMS methods is only moderate. The results for the ECH and the PMS methods are very similar, the correlation ρ between ECH and PMS scales is almost 1. In the case of the BLM method the χ^2/n_{df} indicates that the individual $\alpha_s(M_{\mathrm{Z}}^2)$ measurements are inconsistent. Moreover, the fits using the scales predicted by the BLM method did not converge at all for the observables $JCEF$, O, ρ_D and D_2^{Geneva}. Figure 11 shows the correlation between the logarithms of the experimentally optimized scales and the logarithms of the scales predicted by the ECH, PMS and the BLM methods. For the ECH and the PMS method there are significant correlations of $\rho = 0.75 \pm 0.11$. In the case of BLM there is a slightly negative correlation of $\rho = -0.34 \pm 0.25$, compatible with zero within 1.5 σ. Our results indicate that the ECH and the PMS methods are useful in the case where an experimental optimization can not be performed, whereas the BLM method does not seem to be suitable for the determination of $\alpha_s(M_{\mathrm{Z}}^2)$.

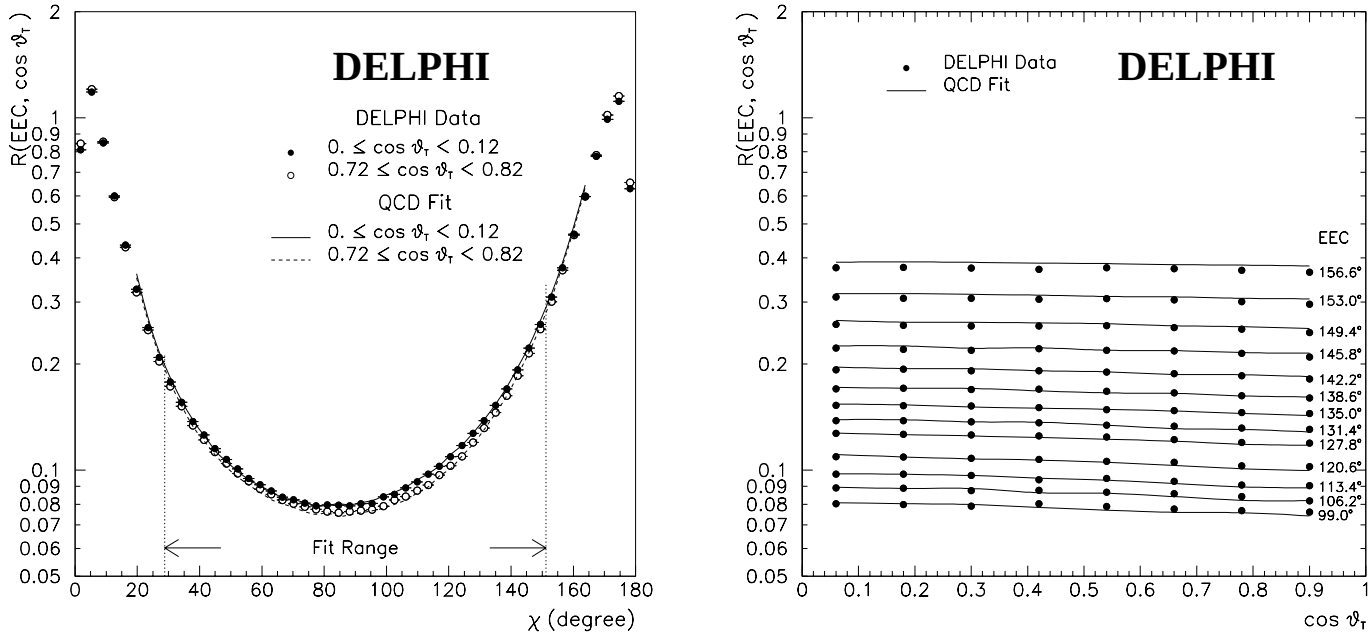

Fig. 8. Same as Fig. 6 but for the energy energy correlation EEC

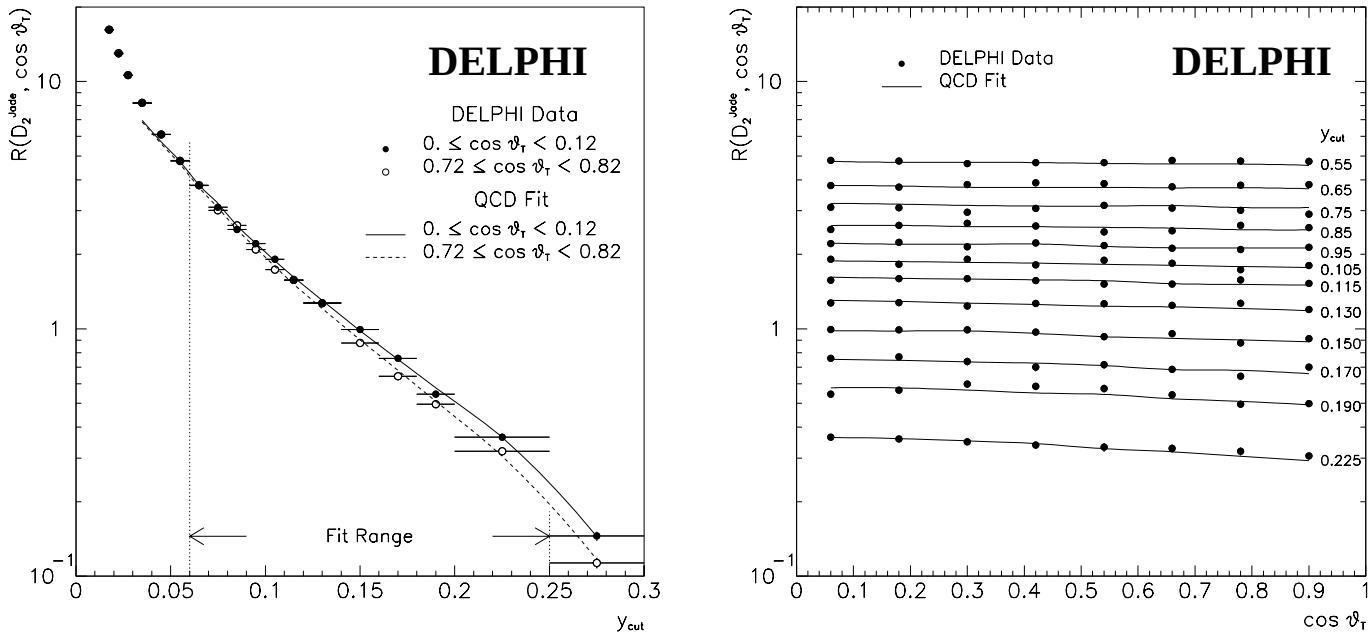

Fig. 9. Same as Fig. 6 but for the differential two jet rate with the Jade Algorithm D_2^{Jade}

6 Padé approximation

An approach for estimating higher-order contributions to a perturbative QCD series is based on Padé Approximations. The Padé Approximant $[N/M]$ to the series

$$S = S_0 + S_1 x + S_2 x^2 + \ldots + S_n x^n \tag{37}$$

is defined [39] by

$$[N/M] \equiv \frac{a_0 + a_1 x + a_2 x^2 + \ldots + a_N x^N}{1 + b_1 x + b_2 x^2 + \ldots + b_M x^M}; \quad N + M = n \tag{38}$$

and

$$[N/M] = S + \mathcal{O}(x^{N+M+1}) \ . \tag{39}$$

The set of (39) can be solved, and by consideration of the terms of $\mathcal{O}(x^{N+M+1})$ one can obtain an estimate of the next order term S_{N+M+1} of the original series. This is called the PA method. Furthermore, for an asymptotic series $[N/M]$ can be taken as an estimate of the sum (PS) of the series to all orders. The PA method has been used successfully to estimate coefficients in statistical physics [39], and various quantum field theories including QCD [40]. Justifications for some of these successes have been

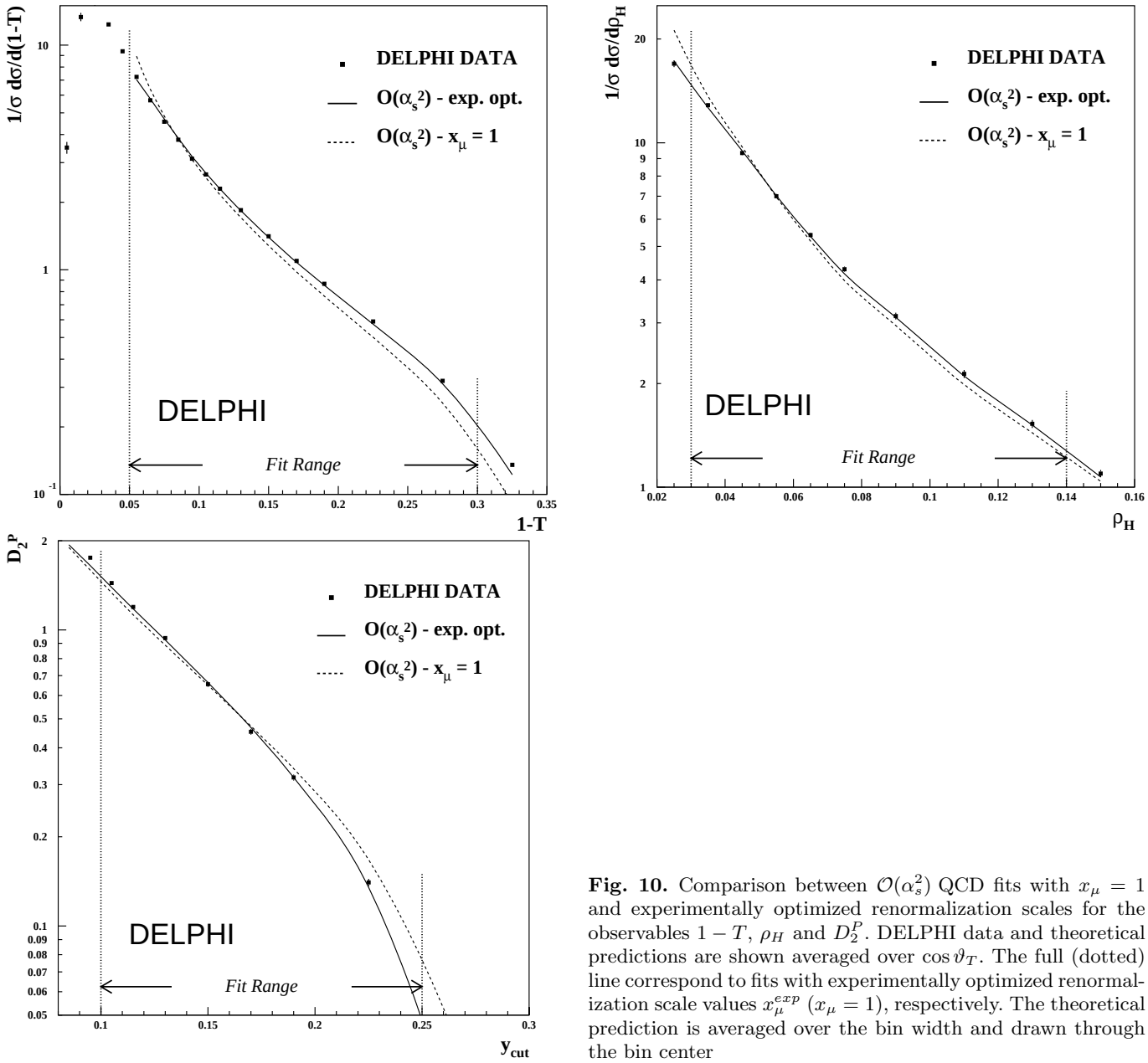

Fig. 10. Comparison between $\mathcal{O}(\alpha_s^2)$ QCD fits with $x_\mu = 1$ and experimentally optimized renormalization scales for the observables $1-T$, ρ_H and D_2^P. DELPHI data and theoretical predictions are shown averaged over $\cos\vartheta_T$. The full (dotted) line correspond to fits with experimentally optimized renormalization scale values x_μ^{exp} ($x_\mu = 1$), respectively. The theoretical prediction is averaged over the bin width and drawn through the bin center

found in mathematical theorems on the convergence and renormalization scale invariance of PAs [40]. In many cases the PAs yield predictions for the higher order coefficients in perturbative series with high accuracy, whereas this accuracy is not expected for the lower order predictions such as $\mathcal{O}(\alpha_s^3)$. For the application of the $\alpha_s(M_Z^2)$ determination from event shapes, the Padé Approximation can serve as a reasonable estimate of the errors due to higher order corrections [41].

For each bin of our observables an estimate for the $\mathcal{O}(\alpha_s^3)$ coefficient $C(y)$ can be derived from [0/1] with $a_0 = A$, $b_1 = -B/A$:

$$C^{Padé}(y) = \frac{B^2(y)}{A(y)}. \qquad (40)$$

It should be noted that the PA predictions $C^{Padé}(y)$ are positive by construction which will result in large errors for kinematical regions where the $\mathcal{O}(\alpha_s^3)$ contribution is negative. The fit range has therefore been determined in the following way: Starting from the same fit range as in $\mathcal{O}(\alpha_s^2)$, the fit has been accepted if $\chi^2/n_{df} \leq 5$. Otherwise the fit range was reduced bin by bin until the fit yielded $\chi^2/n_{df} \leq 5$.

In addition to the $\mathcal{O}(\alpha_s^3)$ fits in the Padé Approximation, the PS method has been used as an estimate of the sum of the perturbative series and $\alpha_s(M_Z^2)$ has been extracted by fitting the [0/1] approximation directly to the data. Here, the fit range has been chosen to be the same as for the fits in the $\mathcal{O}(\alpha_s^3)$ Padé approximation. The χ^2

Table 4. Comparison of the $\alpha_s(M_Z^2)$ values obtained using the different methods for evaluating the renormalization scale suggested by theory. For each observable the $\alpha_s(M_Z^2)$ values using experimentally optimized scales and $\alpha_s(M_Z^2)$ values for the scales predicted by the PMS, ECH and BLM methods are shown. The errors for the $\alpha_s(M_Z^2)$ measurements are assumed to be identical for all methods (see Table 2). The weighted averages are calculated using $\rho_{\rm eff} = 0.635$ and scaling the errors to yield $\chi^2/n_{df} = 1$ in the case of the PMS, ECH and the BLM methods (see text). The χ^2 given for the averaging correspond to the values before adjusting $\rho_{\rm eff}$ and rescaling the measurement uncertainties. The fits using the scales predicted by BLM did not converge for the observables JCEF, O, ρ_D and D_2^{Geneva}

Observable	$\alpha_s^{EXP}(M_Z^2)$	$\alpha_s^{PMS}(M_Z^2)$	$\alpha_s^{ECH}(M_Z^2)$	$\alpha_s^{BLM}(M_Z^2)$
EEC	0.1142	0.1133	0.1135	0.1142
AEEC	0.1150	0.1063	0.1064	0.1179
JCEF	0.1169	0.1168	0.1169	
$1-\mathrm{T}$	0.1132	0.1101	0.1111	0.1133
O	0.1171	0.1128	0.1124	
C	0.1153	0.1119	0.1124	0.1144
$\mathrm{B_{Max}}$	0.1215	0.1222	0.1217	0.1268
$\mathrm{B_{Sum}}$	0.1138	0.1023	0.1021	0.1118
ρ_{H}	0.1215	0.1197	0.1198	0.1258
ρ_{S}	0.1161	0.1154	0.1149	0.1169
ρ_{D}	0.1172	0.1190	0.1203	
$\mathrm{D_2^{E0}}$	0.1165	0.1145	0.1142	0.1143
$\mathrm{D_2^{P0}}$	0.1210	0.1204	0.1202	0.1232
$\mathrm{D_2^{P}}$	0.1187	0.1110	0.1108	0.1118
$\mathrm{D_2^{Jade}}$	0.1169	0.1137	0.1134	0.1137
$\mathrm{D_2^{Durham}}$	0.1169	0.1162	0.1159	0.1241
$\mathrm{D_2^{Geneva}}$	0.1178	0.1064	0.1171	
$\mathrm{D_2^{Cambridge}}$	0.1164	0.1164	0.1163	0.1124
w. average	0.1168 ± 0.0026	0.1154 ± 0.0045	0.1155 ± 0.0044	0.1174 ± 0.0068
χ^2/n_{df}	6.2 / 17	19 / 17	19 / 17	29 / 13

dependence of the $\alpha_s(M_Z^2)$ fits applying the Padé Approximation as a function of the renormalization scale value x_μ is quite small, especially for the PS method. For most of the observables $\alpha_s(M_Z^2)$ and x_μ could not be determined in a simultaneous fit. Therefore, the fits have been done choosing a fixed renormalization scale value $x_\mu = 1$. The uncertainty due to the scale dependence of $\alpha_s(M_Z^2)$ has been estimated by varying x_μ between 0.5 and 2.

The fit results for the individual observables are listed in Tables 5 and 6. The fit applying PS to the B_{Sum} distribution did not converge for any fit range chosen. For the D_2^{Geneva} distribution, the fits did not converge for either method. Comparing the fit results of the $\mathcal{O}(\alpha_s^3)$ fits in Padé Approximation with the fit results in $\mathcal{O}(\alpha_s^2)$ applying $x_\mu = 1$, as given in Table 3 , the scale dependence of $\alpha_s(M_Z^2)$ is reduced for most of the observables, as one would expect from measurements using exact calculations in $\mathcal{O}(\alpha_s^3)$. For the PS method, the reduction of the scale dependence is even larger. Here, $\alpha_s(M_Z^2)$ is less scale dependent than in the $\mathcal{O}(\alpha_s^2)$ fits for all observables considered. Figure 12 shows the scale dependence of $\alpha_s(M_Z^2)$ applying the different QCD predictions to the distribution of the Jet Cone Energy Fraction as an example. There is almost no χ^2 dependence of the $\alpha_s(M_Z^2)$ fits as a function of the renormalization scale for the PS prediction. For the fits applying $\mathcal{O}(\alpha_s^3)$ in the Padé Approximation, the χ^2 dependence is less than for the $\mathcal{O}(\alpha_s^2)$ prediction. However, the JCEF is one of the few observables, where a simultaneous fit of $\alpha_s(M_Z^2)$ and x_μ is possible.

Assuming the same correlation as in the $\mathcal{O}(\alpha_s^2)$ fits, the weighted averages of $\alpha_s(M_Z^2)$ over the observables used have been calculated as:

$$\alpha_{\mathrm{s}}(\mathrm{M_Z^2}) = 0.1168 \pm 0.0054$$

for the PA fits and

$$\alpha_{\mathrm{s}}(\mathrm{M_Z^2}) = 0.1157 \pm 0.0037$$

for the PS fits. The averages are in excellent agreement with the $\mathcal{O}(\alpha_s^2)$ value of $\alpha_{\mathrm{s}}(\mathrm{M_Z^2}) = 0.1168 \pm 0.0026$ using optimized scales. The scatter between the observables, however, is somewhat larger than in the $\mathcal{O}(\alpha_s^2)$ case. The χ^2/n_{df} for the average values is 30/16 and 17/15 respectively.

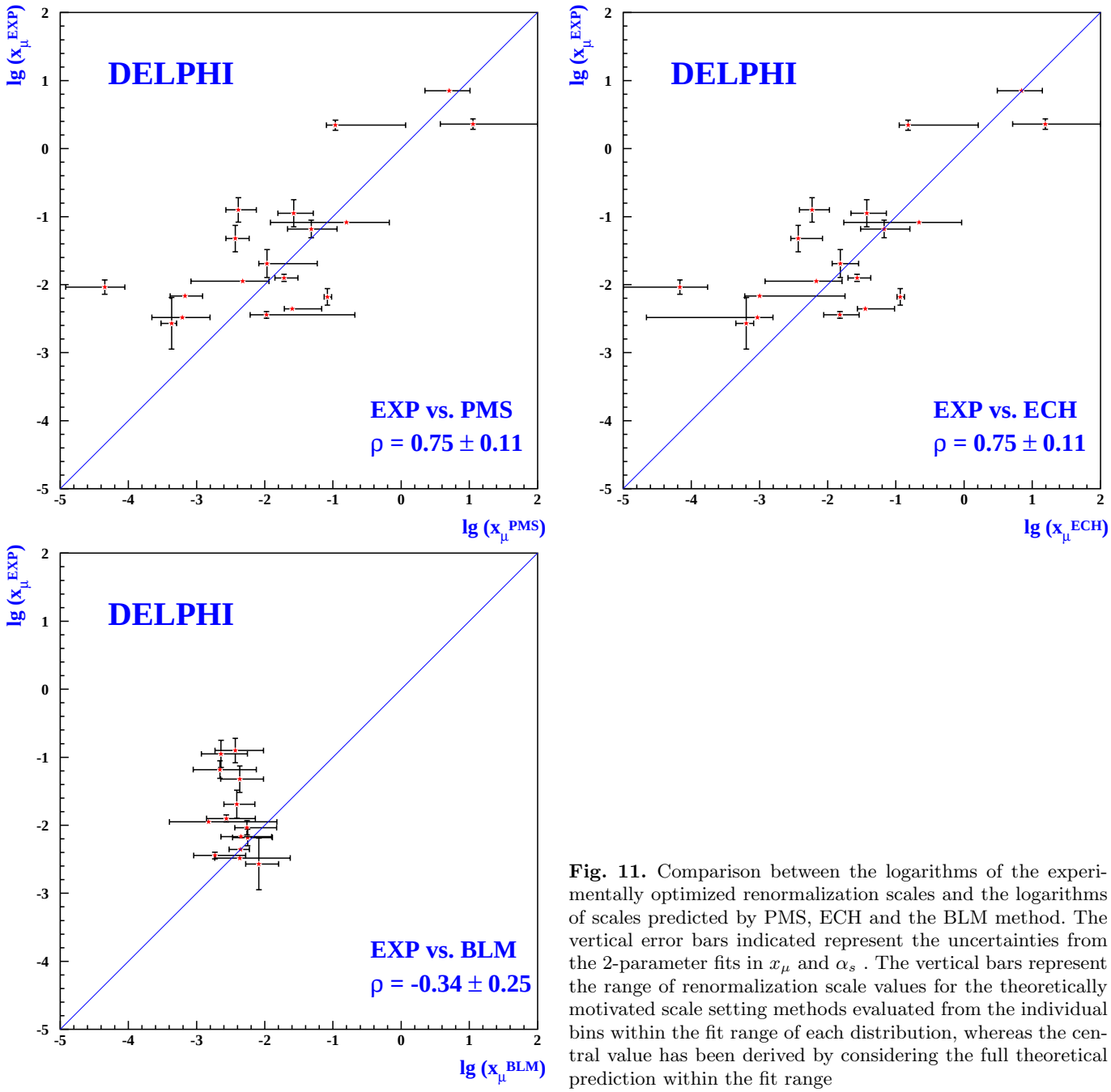

Fig. 11. Comparison between the logarithms of the experimentally optimized renormalization scales and the logarithms of scales predicted by PMS, ECH and the BLM method. The vertical error bars indicated represent the uncertainties from the 2-parameter fits in x_μ and α_s . The vertical bars represent the range of renormalization scale values for the theoretically motivated scale setting methods evaluated from the individual bins within the fit range of each distribution, whereas the central value has been derived by considering the full theoretical prediction within the fit range

7 QCD in the next-to-leading log approximation

All orders resummed QCD calculations in the Next-to-Leading Log Approximation (NLLA) matched with $\mathcal{O}(\alpha_s^2)$ calculations have been used widely to measure $\alpha_s(M_Z^2)$ from event shape observables [3,30].

For a generic event shape observable Y for which the theoretical prediction can be exponentiated, the cumulative cross-section at the scale $Q^2 \equiv s$ is defined by:

$$R(Y,\alpha_s) = \frac{1}{\sigma}\int_0^Y \frac{d\sigma}{dY'}dY' \qquad (41)$$

and can be expanded in the form

$$R(Y,\alpha_s) = C(\alpha_s)\exp\Sigma(\alpha_s,L) + F(\alpha_s,Y) \ , \qquad (42)$$

where $L \equiv \ln(1/Y)$ and

$$C(\alpha_s) = 1 + \sum_{i=1}^{\infty} C_i \bar{\alpha}_s^i \qquad (43)$$

Table 5. Results on $\alpha_s(M_Z^2)$ for QCD-Fits including the $\mathcal{O}(\alpha_s^3)$ Term in the Padé Approximation (PA). For each of the observables the fit range, $\alpha_s(M_Z^2)$, the uncertainty due to scale variation between $0.5 \leq x_\mu \leq 2$ and the total uncertainty are shown. The experimental errors and the uncertainties due to the hadronization corrections are assumed to be the same as for the $\mathcal{O}(\alpha_s^2)$ measurements. The weighted average is calculated using $\rho_{\text{eff}} = 0.635$ and scaling the errors to yield $\chi^2/n_{df} = 1$ (see text). The χ^2 given for the averaging corresponds to the value before adjusting ρ_{eff} and rescaling the measurement uncertainties. The fit for D_2^{Geneva} did not converge

Observable	Fit Range	$\alpha_s(M_Z^2)$	$\Delta\alpha_s$ (Scale.)	$\Delta\alpha_s$ (Tot.)
EEC	$28.8^\circ - 151.2^\circ$	0.1189	± 0.0016	± 0.0026
AEEC	$25.2^\circ - 64.8^\circ$	0.1074	± 0.0030	± 0.0056
JCEF	$104.4^\circ - 169.2^\circ$	0.1169	± 0.0006	± 0.0016
$1-\mathrm{T}$	0.07 - 0.30	0.1207	± 0.0023	± 0.0036
O	0.24 - 0.32	0.1098	± 0.0014	± 0.0044
C	0.32 - 0.72	0.1208	± 0.0023	± 0.0039
$\mathrm{B_{Max}}$	0.10 - 0.24	0.1183	± 0.0016	± 0.0042
$\mathrm{B_{Sum}}$	0.14 - 0.18	0.1127	± 0.0016	± 0.0068
ρ_{H}	0.03 - 0.14	0.1230	± 0.0015	± 0.0036
ρ_{S}	0.10 - 0.30	0.1252	± 0.0024	± 0.0038
ρ_{D}	0.07 - 0.30	0.1045	± 0.0015	± 0.0040
$\mathrm{D_2^{E0}}$	0.05 - 0.18	0.1159	± 0.0014	± 0.0042
$\mathrm{D_2^{P0}}$	0.05 - 0.18	0.1199	± 0.0011	± 0.0034
$\mathrm{D_2^{P}}$	0.10 - 0.20	0.1128	± 0.0008	± 0.0030
$\mathrm{D_2^{Jade}}$	0.06 - 0.25	0.1142	± 0.0014	± 0.0032
$\mathrm{D_2^{Durham}}$	0.015 - 0.16	0.1170	± 0.0009	± 0.0023
$\mathrm{D_2^{Cambridge}}$	0.011 - 0.18	0.1164	± 0.0007	± 0.0026
average		0.1168 ± 0.0054	$\chi^2/n_{df} = 30 \ / \ 16$	

$$\Sigma(\alpha_s, L) = \sum_{i=1}^{\infty} \bar{\alpha}_s^i \sum_{j=1}^{i+1} G_{ij} L^m \tag{44}$$

$$F(\alpha_s, Y) = \sum_{i=1}^{\infty} F_i(Y) \bar{\alpha}_s^i \ . \tag{45}$$

The C_i are constant and the $F_i(Y)$ vanish in the infrared limit $Y \to 0$. The factor Σ to be exponentiated can be written

$$\Sigma(\alpha_s, L) = L f_{LL}(\alpha_s L) + f_{NLL}(\alpha_s L) + \text{subleading terms} \ , \tag{46}$$

where f_{LL} and f_{NLL} represent the leading and the next-to-leading logarithms. They have been calculated for a number of observables, including $1-T$ [42], C [43], B_{max}[44], B_{sum}[44], ρ_H [45] and D_2^{Durham} [46], where the NLLA predictions for B_{max} and B_{sum} entering into this analysis are the recently improved calculations by Yu. L. Dokshitzer et al. [47].

Pure NLLA calculations can be used to measure $\alpha_s(M_Z^2)$ in a limited kinematic region close to the infrared limit, where L becomes large. In order to achieve a prediction where the kinematical range can be extended towards the 3 jet region, several procedures have been suggested [48] to match the NLLA calculations with the calculations in $\mathcal{O}(\alpha_s^2)$.

The $\mathcal{O}(\alpha_s^2)$ QCD formula can be written in the integrated form:

$$R_{\mathcal{O}(\alpha_s^2)}(Y, \alpha_s) = 1 + \mathcal{A}(Y)\bar{\alpha}_s + \mathcal{B}(Y)\bar{\alpha}_s^2 \ , \tag{47}$$

where $\mathcal{A}\ (Y)$ and $\mathcal{B}\ (Y)$ are the cumulative forms of $A(Y, \cos\vartheta_T)$ and $B(Y, \cos\vartheta_T)$ in (28), integrated over ϑ_T. Together with the first and second order part of (44)

$$g_1(L) = G_{12} L^2 + G_{11} L \tag{48}$$

$$g_2(L) = G_{23} L^3 + G_{22} L^2 + G_{21} L \ , \tag{49}$$

the $\ln R$ matching scheme can be defined as:

$$\ln R(Y, \alpha_s) = \Sigma(\alpha_s, L) + H_1(Y)\bar{\alpha}_s + H_2(Y)\bar{\alpha}_s^2 \ , \tag{50}$$

where

$$H_1(Y) = \mathcal{A}(Y) - g_1(L) \tag{51}$$

$$H_2(Y) = \mathcal{B}(Y) - \frac{1}{2}\mathcal{A}^2(Y) - g_2(L). \tag{52}$$

Table 6. Results on $\alpha_s(M_Z^2)$ for QCD-Fits applying the Padé Sum Approximation (PS). For each of the observables $\alpha_s(M_Z^2)$, the uncertainty due to scale variation between $0.5 \leq x_\mu \leq 2$ and the total uncertainty are shown. The experimental errors and the uncertainties due to the hadronization corrections are assumed to be the same as for the $\mathcal{O}(\alpha_s^2)$ measurements. The weighted average is calculated using $\rho_{\text{eff}} = 0.635$ and scaling the errors to yield $\chi^2/n_{df} = 1$ (see text). The χ^2 given for the averaging corresponds to the value before adjusting ρ_{eff} and rescaling the measurement uncertainties. The fits for B_{Sum} and D_2^{Geneva} did not converge

Observable	$\alpha_s(M_Z^2)$	$\Delta\alpha_s$ (Scale.)	$\Delta\alpha_s$ (Tot.)
EEC	0.1147	$\pm$0.0003	$\pm$0.0021
AEEC	0.1070	$\pm$0.0002	$\pm$0.0048
JCEF	0.1169	$\pm$0.0003	$\pm$0.0015
1 − T	0.1165	$\pm$0.0003	$\pm$0.0028
O	0.1135	$\pm$0.0003	$\pm$0.0042
C	0.1150	$\pm$0.0003	$\pm$0.0032
B_{Max}	0.1196	$\pm$0.0003	$\pm$0.0039
ρ_H	0.1219	$\pm$0.0004	$\pm$0.0033
ρ_S	0.1161	$\pm$0.0003	$\pm$0.0029
ρ_D	0.1098	$\pm$0.0003	$\pm$0.0037
D_2^{E0}	0.1136	$\pm$0.0003	$\pm$0.0040
D_2^{P0}	0.1198	$\pm$0.0003	$\pm$0.0032
D_2^{P}	0.1124	$\pm$0.0003	$\pm$0.0029
D_2^{Jade}	0.1123	$\pm$0.0003	$\pm$0.0029
D_2^{Durham}	0.1164	$\pm$0.0003	$\pm$0.0021
$D_2^{Cambridge}$	0.1162	$\pm$0.0003	$\pm$0.0025
average	0.1157 ± 0.0037	$\chi^2/n_{df} = 17\ /\ 15$	

When combining $\mathcal{O}(\alpha_s^2)$ predictions with NLLA calculations one has to take into account that the resummed terms do not vanish at the upper kinematic limit Y_{max} of the event shape distributions. In order to correct for this, the resummed logarithms are redefined [49] by:

$$L = \ln(1/Y - 1/Y_{max} + 1). \tag{53}$$

Several other matching schemes can be defined which differ in the treatment of the subleading terms, thus introducing a principal ambiguity in the matching procedure. The $\ln R$ matching scheme has become the preferred one, because it includes the C_2 and the G_{21} coefficients implicitly and uses only those NLLA terms which are known analytically. It yields the best description of the data in terms of χ^2/n_{df} in most cases [3]. Therefore, we quote the results for the matched predictions using the $\ln R$ matching scheme and use the R and $R - G_{21}$ matching schemes as defined e.g. in [3] for the estimation of the uncertainty due to the matching ambiguity.

7.1 Measurement of $\alpha_s(M_Z^2)$ using pure NLLA predictions

To measure $\alpha_s(M_Z^2)$ from pure NLLA calculations the fit range has to be restricted to the extreme 2-jet region,

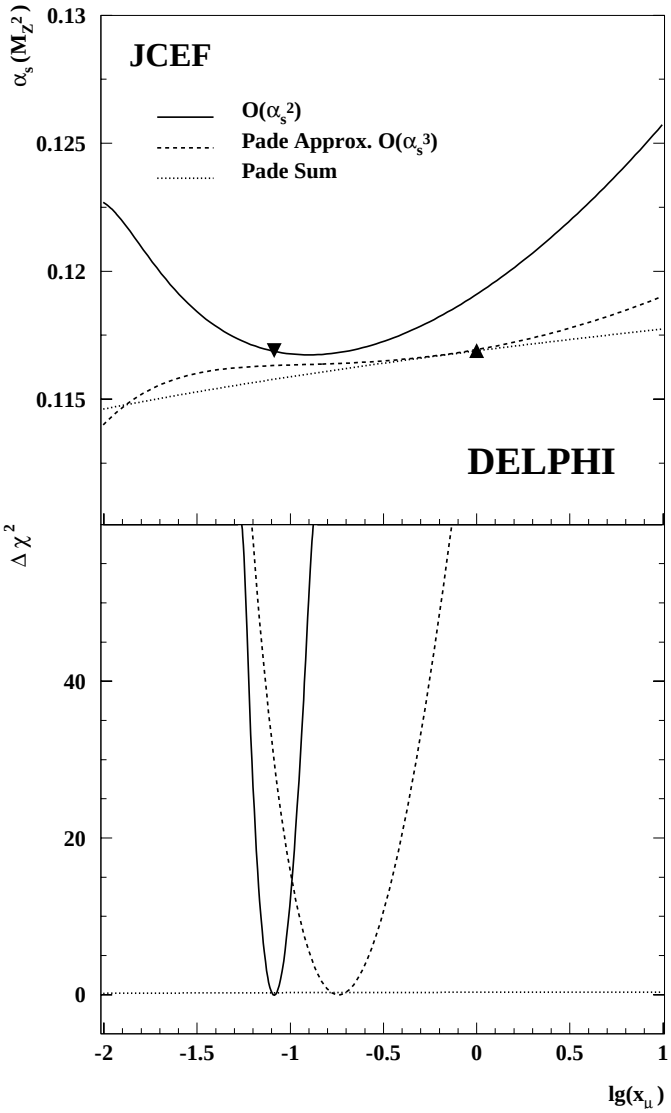

Fig. 12. $\alpha_s(M_Z^2)$ and $\Delta\chi^2 = \chi^2 - \chi^2_{\text{min}}$ for the distribution of the Jet Cone Energy Fraction as a function of x_μ from QCD fits applying $\mathcal{O}(\alpha_s^2)$ prediction, $\mathcal{O}(\alpha_s^3)$ in Padé Approximation and the Padé Sum Approximation. Additionally, the χ^2 minimum for the $\mathcal{O}(\alpha_s^2)$ fit and the renormalization scale value $x_\mu = 1$ have been indicated in the $\alpha_s(M_Z^2)$ curves

where L becomes large and the resummed logarithms dominate. We define ω as the ratio of the resummed logarithms to the non-exponentiating second order contributions as follows:

$$\omega = \frac{\Sigma(\alpha_s, L)}{H_1(Y)\bar{\alpha}_s + H_2(Y)\bar{\alpha}_s^2} \tag{54}$$

In addition to the fit range criteria listed in Sect. 4 we require the minimum of the ratio ω over the fit range not to fall below 5 for the fits in pure NLLA. This leads to the fit ranges listed in Table 7. For the observable D_2^{Durham} the ratio ω remains small even for small values of y_{cut}. No fit range can be found where the resummed logarithms dominate the prediction. Therefore D_2^{Durham} has not been used for the fits in pure NLLA.

Table 7. Fit range for the observables in pure NLLA and matched NLLA fits. The observable D_2^{Durham} has not been used for pure NLLA fits, since no fit range can be found, where the resummed logarithms dominate the predictions (see text)

Observable	Fit Range (NLLA)	Fit Range (matched)
$1-\mathrm{T}$	0.04 - 0.09	0.04 - 0.30
C	0.08 - 0.16	0.08 - 0.72
$\mathrm{B_{max}}$	0.02 - 0.04	0.02 - 0.24
$\mathrm{B_{sum}}$	0.06 - 0.08	0.06 - 0.24
ρ_{H}	0.03 - 0.06	0.03 - 0.30
$\mathrm{D_2^{Durham}}$		0.015 - 0.16

Contrary to the $\mathcal{O}(\alpha_s^2)$ predictions an optimization of the renormalization scale (or more precisely an optimization of the renormalization scheme) cannot be easily performed for the resummed NLLA predictions [4]. Therefore the scale was fixed to $x_\mu = 1$. The uncertainty due to the scale dependence of $\alpha_s(M_Z^2)$ was estimated by varying the scale x_μ between 0.5 and 2.

The fit results for the individual observables are listed in Table 8. The weighted average of $\alpha_s(M_Z^2)$ for the 5 observables is

$$\alpha_s(M_Z^2) \ = 0.116 \pm 0.006$$

which is in excellent agreement with the average value for the $\mathcal{O}(\alpha_s^2)$ fits of $\alpha_s(M_Z^2) = 0.1168 \pm 0.0026$.

7.2 Measurement of $\alpha_s(M_Z^2)$ using NLLA predictions matched with $\mathcal{O}(\alpha_s^2)$

For the QCD fits using NLLA theory matched with $\mathcal{O}(\alpha_s^2)$ predictions the fit range has been chosen as the combined fit range for the pure NLLA and the $\mathcal{O}(\alpha_s^2)$ fits. The results for the individual observables in the $\ln R$ matching scheme are listed in Table 9. The additional uncertainty due to the matching ambiguity has been estimated as the maximum difference of $\alpha_s(M_Z^2)$ in the $\ln R$ matching scheme and the two alternative matching schemes, R and $R - G_{21}$. The dependence on the choice of Y_{max}, i.e. the value of the upper kinematic limit for the shape observables used for the redefinition of the resummed logarithms according to (53), has been studied by repeating the fits with the value of Y_{max} being reduced by 10 %. The resulting variation in $\alpha_s(M_Z^2)$ has been found to be small, the maximum change is about 1 %.

The average value of $\alpha_s(M_Z^2)$ in the $\ln R$ matching scheme is

$$\alpha_s(M_Z^2) \ = 0.119 \pm 0.005$$

which is in good agreement with the average value for the $\mathcal{O}(\alpha_s^2)$ fits of $\alpha_s(M_Z^2) = 0.1168 \pm 0.0026$.

Looking at the individual fit results, one finds from the χ^2/n_{df} that most of the shape distributions cannot be successfully described in a fit range expected to apply for the combined theory. The $\alpha_s(M_Z^2)$ values are higher than for the fits in pure NLLA for all observables considered. In the case of $1-T$, C and B_{sum} the measured $\alpha_s(M_Z^2)$ values are even above the values for both the pure NLLA fits and the $\mathcal{O}(\alpha_s^2)$ fits using experimentally optimized scales, where one naively might expect the matched predictions to be a kind of 'average' of the individual theories.

In order to investigate this result further it is instructive to compare the theoretical predictions of the shape distributions for the different methods with the data distributions. Figure 13 shows experimental distributions for $1-T$ and C in comparison with the fitted curves for three different types of QCD fits, namely $\mathcal{O}(\alpha_s^2)$ using experimentally optimized scales, $\mathcal{O}(\alpha_s^2)$ using a fixed renormalization scale $x_\mu = 1$ and the fits in the $\ln R$ matching scheme. For the fits in $\mathcal{O}(\alpha_s^2)$ using experimentally optimized scales, the data are described well over the whole fit range. For the fits in $\mathcal{O}(\alpha_s^2)$ using a fixed renormalization scale and the fits in the $\ln R$ matching scheme, we find only a poor description and the slope of both curves show a similar systematic distortion with respect to the data. In the case of $\mathcal{O}(\alpha_s^2)$ applying $x_\mu = 1$ the distortion arises from the wrong choice of the renormalization scale. Since the scale value for the matched predictions is also chosen to be $x_\mu = 1$, the similarity of the curves indicates that the subleading and non-logarithmic terms originating from the $\mathcal{O}(\alpha_s^2)$ part of the matched theory and introduced using the scale value $x_\mu = 1$ dominate the $\ln R$ predictions. It should be noted that the matched theory requires a renormalization scale value of $\mathcal{O}$ (1). Unlike the $\mathcal{O}(\alpha_s^2)$ case, 2 parameter fits in $\alpha_s(M_Z^2)$ and x_μ do not converge for most of the observables; for such low scale values as in $\mathcal{O}(\alpha_s^2)$ the data can not be described at all in the matched theory. It seems that the combination of all orders resummed predictions and terms only known in $\mathcal{O}(\alpha_s^2)$ results in a systematic shift in $\alpha_s(M_Z^2)$ due to the impossibility of choosing an appropriate renormalization scale value. Although the average values for the $\mathcal{O}(\alpha_s^2)$ fits, the fits in pure NLLA and the fits in the $\ln R$ matching scheme are in good agreement, the matched results should be considered to be less reliable than those of the $\mathcal{O}(\alpha_s^2)$ and pure NLLA analyses due to the systematic deviation of the prediction to most of the data distributions (see e.g. Fig. 13 and Table 9).

8 Heavy quark mass effects

Studies of the influence of quark mass effects on jet cross-sections [50] have shown that these effects can be important in the study of event shape observables and hence in the measurement of the strong coupling. For a natural mixture of quark flavours, the influence of the quark masses on the measurement of $\alpha_s(M_Z^2)$ from event shapes is expected to be $\sim 1\%$ [51]. In order to derive a high precision value of $\alpha_s(M_Z^2)$, the $\mathcal{O}(\alpha_s^2)$ measurement with experimentally optimized scales has been refined by considering the influence of b quark mass effects in leading

Table 8. Results for the $\alpha_s(M_Z^2)$ fits in pure NLLA for the individual observables together with the individual sources of uncertainties and the χ^2/n_{df} for the NLLA fits. The total error on $\alpha_s(M_Z^2)$ listed, is the quadratic sum of the experimental error (statistical and systematic uncertainty), the uncertainty due to the hadronization correction and the uncertainty due to the scale dependence of $\alpha_s(M_Z^2)$. Also listed is the weighted average of $\alpha_s(M_Z^2)$ for the 5 observables together with the χ^2/n_{df} for the averaging procedure and the correlation parameter $\rho_{\rm eff}$. The χ^2 corresponds to the value before readjusting according to (33)

Observable	$\alpha_s(M_Z^2)$	$\Delta\alpha_s$ (exp.)	$\Delta\alpha_s$ (had.)	$\Delta\alpha_s$ (scal.)	$\Delta\alpha_s$ (tot.)	χ^2/n_{df}
$1-\mathrm{T}$	0.120	±0.001	±0.004	±0.004	±0.006	0.59
C	0.116	±0.002	±0.003	±0.004	±0.006	0.53
$\mathrm{B_{max}}$	0.111	±0.004	±0.003	±0.002	±0.006	2.37
$\mathrm{B_{sum}}$	0.116	±0.003	±0.004	±0.002	±0.006	1.24
$\rho_{\rm H}$	0.117	±0.004	±0.006	±0.004	±0.009	0.43
average	0.116 ± 0.006		$\chi^2/n_{df} = 1.2\ /\ 4$	$\rho_{\rm eff} = 0.71$		

Table 9. Results of the QCD fits in the $\ln R$ matching scheme for the individual observables together with the individual sources of uncertainties and the χ^2/n_{df} for the $\alpha_s(M_Z^2)$ fits. The total error is the quadratic sum of the experimental error (statistical and systematic uncertainty), the uncertainty due to the hadronization correction, the uncertainty due to the scale dependence of $\alpha_s(M_Z^2)$ and the uncertainty due to the matching ambiguity. Also listed is the weighted average of $\alpha_s(M_Z^2)$ for the 6 observables together with the χ^2/n_{df} for the averaging procedure and the correlation parameter $\rho_{\rm eff}$. The χ^2 corresponds to the value before readjusting according to (33)

Observable	$\alpha_s(M_Z^2)$	$\Delta\alpha_s$ (exp.)	$\Delta\alpha_s$ (had.)	$\Delta\alpha_s$ (scal.)	$\Delta\alpha_s$ (mat.)	$\Delta\alpha_s$ (tot.)	χ^2/n_{df}
$1-\mathrm{T}$	0.124	±0.002	±0.003	±0.004	±0.003	±0.007	9.5
C	0.120	±0.002	±0.002	±0.004	±0.004	±0.007	15.2
$\mathrm{B_{max}}$	0.113	±0.002	±0.002	±0.003	±0.003	±0.005	8.4
$\mathrm{B_{sum}}$	0.122	±0.002	±0.003	±0.004	±0.005	±0.008	11.9
$\rho_{\rm H}$	0.119	±0.002	±0.002	±0.003	±0.005	±0.007	1.33
$\mathrm{D_2^{Durham}}$	0.121	±0.001	±0.002	±0.002	±0.005	±0.006	1.70
average	0.119 ± 0.005		$\chi^2/n_{df} = 2.3\ /\ 5$		$\rho_{\rm eff} = 0.57$		

order:

$$\frac{1}{\sigma_{tot}}\frac{d^2\sigma(Y,\cos\vartheta_T)}{dY\,d\cos\vartheta_T} = \bar{\alpha}_s(\mu^2)\cdot A(Y,\cos\vartheta_T)\big[1+\Delta m\big] + \bar{\alpha_s}^2(\mu^2)\cdot B(Y,\cos\vartheta_T,x_\mu) \quad (55)$$

where

$$\Delta m = \frac{\sum\limits_{q,m_b\neq0} d^2\sigma_q(Y,\cos\theta_T)/\sum\limits_{q,m_b\neq0}\sigma_q}{\sum\limits_{q,m_b=0} d^2\sigma_q(Y,\cos\theta_T)/\sum\limits_{q,m_b=0}\sigma_q} - 1 \quad (56)$$

The coefficients Δm for the 18 observables studied have been computed numerically [52] for two different definitions of the b-quark mass: The b pole mass of $M_b \approx 4.6\ \mathrm{GeV/c^2}$ and the b running mass at the M_Z, $m_b(M_Z) \approx 2.8\ \mathrm{GeV/c^2}$ [50]. All definitions of the quark mass are equivalent to leading order; differences are entirely due to higher orders in α_s. $\alpha_s(M_Z^2)$ has been determined applying both mass definitions. The average of $\alpha_s(M_Z^2)$ derived from the pole mass definition and the running mass definition has been taken as the central value, and half the difference has been taken as an estimate of the uncertainty due to higher order mass effects. The results for the individual observables are listed in Table 10.

9 Summary

From 1.4 Million hadronic $\mathrm{Z_0}$ decays recorded with the DELPHI detector and reprocessed with improved analysis software, the distributions of 18 infrared and collinear safe observables have been precisely measured at various values of the polar angle $\vartheta_{\rm T}$ of the thrust axis with respect to the beam direction. The $\vartheta_{\rm T}$ dependence of all detector properties has been taken fully into account to achieve the best possible experimental precision. In order to compare with QCD calculations in $\mathcal{O}(\alpha_s^2)$, hadronization corrections are evaluated from precisely tuned fragmentation models.

The precise data are used to measure $\alpha_s(M_Z^2)$ applying a number of different methods described in the literature. The most detailed studies have been performed in second order pertubative QCD. Fits taking explicit account of

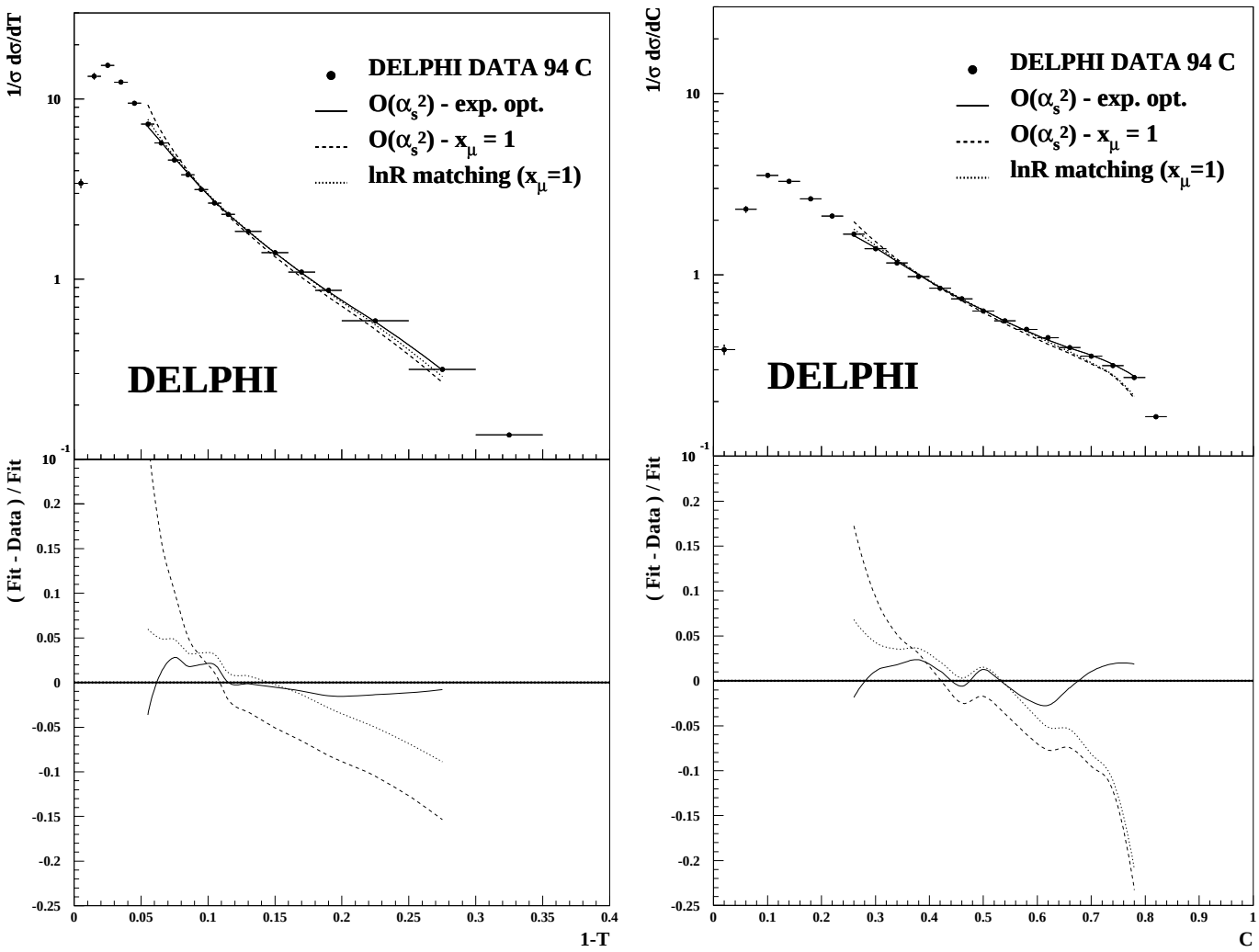

Fig. 13. *Left part:* Comparison of DELPHI data with three different QCD Fits: *i*) $\mathcal{O}(\alpha_s^2)$ using an experimentally optimized renormalization scale, *ii*) $\mathcal{O}(\alpha_s^2)$ using a fixed renormalization scale $x_\mu = 1$ and *iii*) $\ln R$ matched NLLA ($x_\mu = 1$) for the thrust Distribution. The lower part shows the relative difference (Fit-Data)/Fit. Whereas the $\mathcal{O}(\alpha_s^2)$ curve describes the data over the whole fit range, the slope of the curves for the fixed scale and $\ln R$ matching show a similar systematic distortion with respect to the data. *Right part:* The same for the C-Parameter. Here the distortion is even stronger

the α_s dependent event orientation as predicted by QCD with experimental acceptance corrections less than $\sim 25\%$ and hadronization corrections less than $\sim 40\%$ yield the result that the data can be surprisingly well described in $\mathcal{O}(\alpha_s^2)$ by using a common value of $\alpha_s(M_Z^2)$ with a small uncertainty.

Taking account of the correlation among the observables an average value of $\alpha_s(M_Z^2) = 0.1168 \pm 0.0026$ is obtained from the data. The consistency of the individual $\alpha_s(M_Z^2)$ determinations from the 18 shape distributions is achieved by using the different values of the renormalization scales as obtained from the individual fits, i.e. applying the so called experimental optimization method. The significance of the fits is improved due to the large number of data points per distribution. Thus, definite results concerning the choice of the optimal renormalization scale value become possible. It should be pointed out that for most of the investigated observables the scale dependence of α_s is very small in the vicinity of the experimentally optimized scale. The quoted error of $\alpha_s(M_Z^2)$ includes the uncertainty due to a variation of the experimentally optimized scale in the range between $0.5 \cdot x_\mu^{exp}$ and $2. \cdot x_\mu^{exp}$.

An analysis with a fixed renormalization scale value of $x_\mu = 1$ yields an unacceptable description of the data for many observables and leads to a wide spread of the $\alpha_s(M_Z^2)$ values. In contrast to fits applying experimentally optimized scales, the stability of $\alpha_s(M_Z^2)$ with respect to the choice of the fit range is in general quite poor. Due to the improved accuracy of the data, systematic differences between the $\mathcal{O}(\alpha_s^2)$ analysis using experimentally optimized and fixed renormalization scale values $x_\mu = 1$ become visible. These differences propagate also into the matched NLLA-analysis.

To check the reliability of the α_s results obtained from the experimentally optimized scales three further approaches for choosing an optimized value of the renor-

Table 10. Results of the refined $\mathcal{O}(\alpha_s^2)$ measurement of $\alpha_s(M_Z^2)$ including b quark mass effects in leading order. The central value of $\alpha_s(M_Z^2)$ quoted is the average of α_s derived from applying the b pole mass M_b and the b running mass $m_b(M_Z)$ definition. $\Delta\alpha_s(Mass) = |\alpha_s(M_b) - \alpha_s(m_b(M_Z))|/2$ has been taken as an estimate of the uncertainty due to quark mass effects of higher orders. The total error displayed is the quadratic sum of the experimental uncertainty, the hadronization uncertainty, the scale uncertainty and the uncertainty due to quark mass effects. The χ^2 given, corresponds to the value before readjusting according to (33)

Observable	$\alpha_s(M_Z^2)$	$\Delta\alpha_s$ (Mass)	$\Delta\alpha_s$ (Tot.)
EEC	0.1145	$\pm$ 0.0001	$\pm$ 0.0028
AEEC	0.1149	$\pm$ 0.0001	$\pm$ 0.0111
JCEF	0.1180	$\pm$ 0.0007	$\pm$ 0.0018
$1-\mathrm{T}$	0.1136	$\pm$ 0.0001	$\pm$ 0.0036
O	0.1184	$\pm$ 0.0006	$\pm$ 0.0057
C	0.1156	$\pm$ 0.0002	$\pm$ 0.0036
$\mathrm{B_{Max}}$	0.1223	$\pm$ 0.0002	$\pm$ 0.0041
$\mathrm{B_{Sum}}$	0.1144	$\pm$ 0.0003	$\pm$ 0.0053
ρ_{H}	0.1216	$\pm$ 0.0001	$\pm$ 0.0060
ρ_{S}	0.1160	$\pm$ 0.0001	$\pm$ 0.0029
ρ_{D}	0.1196	$\pm$ 0.0008	$\pm$ 0.0039
$\mathrm{D_2^{E0}}$	0.1165	$\pm$ 0.0002	$\pm$ 0.0044
$\mathrm{D_2^{P0}}$	0.1207	$\pm$ 0.0002	$\pm$ 0.0033
$\mathrm{D_2^{P}}$	0.1186	$\pm$ 0.0001	$\pm$ 0.0046
$\mathrm{D_2^{Jade}}$	0.1182	$\pm$ 0.0005	$\pm$ 0.0041
$\mathrm{D_2^{Durham}}$	0.1172	$\pm$ 0.0003	$\pm$ 0.0026
$\mathrm{D_2^{Geneva}}$	0.1216	$\pm$ 0.0013	$\pm$ 0.0310
$\mathrm{D_2^{Cambridge}}$	0.1176	$\pm$ 0.0006	$\pm$ 0.0026
average	0.1174 ± 0.0026	$\chi^2/n_{df} = 6.60/17$	$\rho_{\mathrm{eff}} = 0.615$

malization scale have been investigated: The principle of minimal sensitivity (PMS), the method of effective charges (ECH), and the method of Brodsky, Lepage and MacKenzie (BLM). The weighted averages of α_s from the three methods are in excellent agreement with the weighted average of α_s obtained from the experimental optimization, but their scatter is larger. The scatter is largest for BLM. A significant correlation between the renormalization scale values evaluated with ECH and PMS with the experimentally optimized scale values is observed. No such correlation exists for the BLM scales.

Further approaches to estimate the influence of higher order contributions to the perturbative QCD series are based on Padé approximants. The [0/1] Padé approximant has been used as an estimate of the sum of the perturbative series as well as for the extrapolation of the unknown $\mathcal{O}(\alpha_s^3)$ coefficients for the 18 distributions. In both studies the renormalization scale has been set to $x_\mu = 1$. Again the average values of $\alpha_s(M_Z^2)$ are consistent with the average value from the experimental scale optimization in $\mathcal{O}(\alpha_s^2)$.

While all above mentioned determinations of $\alpha_s(M_Z^2)$ use fixed order perturbation theory the last part of the paper describes measurements of $\alpha_s(M_Z^2)$ using all orders resummed calculations in the next-to-leading logarithmic approximation (NLLA). In a first step, pure NLLA predictions have been confronted with the data in a limited fit range where the ratio of the resummed next-to-leading logarithms to the non-exponentiating $\mathcal{O}(\alpha_s^2)$ contributions is large. The very good agreement between the average value of $\alpha_s(M_Z^2)$ obtained from the pure NLLA fits with a renormalization scale value $x_\mu = 1$ and the $\mathcal{O}(\alpha_s^2)$ fits using experimentally optimized scales is remarkable. In a further step NLLA matched to $\mathcal{O}(\alpha_s^2)$ calculations have been applied. The corresponding average value of $\alpha_s(M_Z^2)$ is again consistent with the $\mathcal{O}(\alpha_s^2)$ result though the α_s values from all investigated observables are systematically higher. More importantly, the application of matched NLLA to the high precision data reveals that the trend of the data deviates in a systematic fashion from the predictions of the matched theory. This problem has not previously been observed. The matched results should be considered to be less reliable than those of the $\mathcal{O}(\alpha_s^2)$ and pure NLLA analyses.

The α_s values derived from the different approaches considered are in very good agreement. The $\mathcal{O}(\alpha_s^2)$ analysis applying a simultaneous fit of α_s and x_μ to the experimental data yields superior results in all respects.

In a final step the influence of heavy quark mass effects on the measurement of $\alpha_s(M_Z^2)$ has been studied. The weighted average of $\alpha_s(M_Z^2)$ from the $\mathcal{O}(\alpha_s^2)$ measurements using experimentally optimized renormalization scale values and corrected for the $b-$mass to leading order yields

$$\alpha_s(M_Z^2) = 0.1174 \pm 0.0026.$$

The result is consistent with the result of a previous DELPHI publication [2] if compared with partonshower hadronization corrections.

Among the observables studied, the Jet Cone Energy Fraction (JCEF) [19] naturally reveals some superior properties. First, the size of the hadronization correction is extremely small, the average correction within the applied fit range being only about 3.5%. Furthermore, the second order contribution to the cross-section is quite small. Within the applied fit range, the average ratio of the second to first order contributions is $\langle r_{NLO}\rangle \sim 25\%$ if x_μ is fixed at 1 and only $\langle r_{NLO}\rangle \sim 6\%$ if the experimentally optimized scale value is applied. This indicates a good convergence behavior of the corresponding perturbative series. Also the scale dependence of $\alpha_s(M_Z^2)$ derived from JCEF is very small. Both experimental and theoretical uncertainties are smallest for the $\alpha_s(M_Z^2)$ measurement from the JCEF distribution.

Table 11 shows a summary of α_s measurements from the JCEF distribution for the different methods. The $\mathcal{O}(\alpha_s^2)$ fit of $\alpha_s(M_Z^2)$ applying a fixed renormalization scale value $x_\mu = 1$ clearly fails to describe the data with $\chi^2/n_{df} = 965/125$. However, even for this method, the deviation of $\alpha_s(M_Z^2)$ from the value obtained using the experimentally optimized scale value is only about 2 %. All other

Table 11. Summary of $\alpha_s(M_Z^2)$ measurements from the distribution of the Jet Cone Energy Fraction (JCEF)

prediction	$\alpha_s(M_Z^2)$	x_μ	χ^2/n_{df}
$\mathcal{O}(\alpha_s^2)$ exp. opt. scale	0.1169 ± 0.0017	0.0820	1.05
ECH/FAC	0.1169 ± 0.0017	0.2189	2.75
PMS	0.1168 ± 0.0017	0.1576	1.91
Padé $\mathcal{O}(\alpha_s^3)$ (fixed scale)	0.1169 ± 0.0016	1.0	3.12
Padé Sum (fixed scale)	0.1169 ± 0.0015	1.0	3.05
Padé $\mathcal{O}(\alpha_s^3)$ (exp. opt. scale)	0.1164 ± 0.0015	0.1814	2.45
$\mathcal{O}(\alpha_s^2)$ (fixed scale)	0.1191 ± 0.0024	1.0	7.7
$\mathcal{O}(\alpha_s^2)$ exp. opt. scale + LO quark mass effects	0.1180 ± 0.0018		

approaches yield nearly identical α_s values within a few per mille. The deviation of the α_s values derived from the different methods, which can serve as an estimate of the theoretical uncertainty due to missing higher order terms [35], is clearly smaller than the uncertainty of ± 0.0008 derived from the variation of the renormalization scale value. Due to the outstanding qualities of this observable, the JCEF is considered as best suited for a precise determination of $\alpha_s(M_Z^2)$. After correcting the measured value for heavy quark mass effects, the final result is

$$\alpha_s(M_Z^2) = 0.1180 \pm 0.0006(\text{exp.}) \pm 0.0013(\text{hadr.}) \\ \pm 0.0008(\text{scale}) \pm 0.0007(\text{mass}).$$

Comparing this result with other recent precision measurements of $\alpha_s(M_Z^2)$, there is very good agreement with the determination of $\alpha_s(M_Z^2) = 0.1174 \pm 0.0024$ from Lattice Gauge Theory [53] and the recent result from an NNLO analysis of *ep* deep inelastic scattering data of $\alpha_s(M_Z^2) = 0.1172 \pm 0.0024$ [54]. The result is also in good agreement with the result from the LEP electroweak working group of $\alpha_s(M_Z^2) = 0.119 \pm 0.004$ [55] from the standard model fit to the full set of electroweak precision data. Compared with the most recent result from spectral functions in hadronic tau decays, α_s is smaller than the central value of $\alpha_s(M_Z^2) = 0.1219 \pm 0.0020$ quoted in [56], but in very good agreement with the value of $\alpha_s(M_Z^2) = 0.1169 \pm 0.0017$ derived in [56] by using an alternative analysis method considering renormalon chains.

Acknowledgements. We thank M. Seymour for providing us with the EVENT2 generator and for useful discussions. We further thank P. Aurenche, S. Catani, J. Ellis and P. Zerwas for critical comments and stimulating discussions. We are greatly indebted to our technical collaborators, to the members of the CERN-SL Division for the excellent performance of the LEP collider, and to the funding agencies for their support in building and operating the DELPHI detector. We acknowledge in particular the support of Austrian Federal Ministry of Science and Traffics, GZ 616.364/2-III/2a/98, FNRS–FWO, Belgium, FINEP, CNPq, CAPES, FUJB and FAPERJ, Brazil, Czech Ministry of Industry and Trade, GA CR 202/96/0450 and GA AVCR A1010521, Danish Natural Research Council, Commission of the European Communities (DG XII), Direction des Sciences de la Matière, CEA, France, Bundesministerium für Bildung, Wissenschaft, Forschung und Technologie, Germany, General Secretariat for Research and Technology, Greece, National Science Foundation (NWO) and Foundation for Research on Matter (FOM), The Netherlands, Norwegian Research Council, State Committee for Scientific Research, Poland, 2P03B06015, 2P03B03311 and SPUB/P03/178/98, JNICT–Junta Nacional de Investigação Científica e Tecnológica, Portugal, Vedecka grantova agentura MS SR, Slovakia, Nr. 95/5195/134, Ministry of Science and Technology of the Republic of Slovenia, CICYT, Spain, AEN96–1661 and AEN96-1681, The Swedish Natural Science Research Council, Particle Physics and Astronomy Research Council, UK, Department of Energy, USA, DE–FG02–94ER40817.

References

1. S. Catani, M. Seymour, Nucl. Phys. B **485** (1997) 291-419
2. DELPHI Collab., P. Abreu et al., Z. Phys. C **54** (1992) 55
3. DELPHI Collab., P. Abreu et al., Z. Phys. C **59** (1993) 21
4. D. T. Barclay, C. J. Maxwell, M. T. Reader, Phys. Rev. D **49** (1994) 3480
5. DELPHI Collab., P. Abreu et al., Nucl. Instr. Meth. A **303** (1991) 233; DELPHI Collab., P. Abreu et al., Nucl. Instr. Meth. A **378** (1996) 57
6. F. Jadach, B.F.L. Ward, Z. Was, Comp. Phys. Comm. **40** (1986) 285; Nucl. Phys. B **253** (1985) 441
7. DELPHI Coll., P. Abreu et al., Nucl. Inst. and Meth. A **378** (1996) 57
8. T. Sjöstrand, Comp. Phys. Comm. **39** (1986) 347; T. Sjöstrand, M. Bengtsson, Comp. Phys. Comm. **46** (1987) 367
9. J.E. Campagne, R. Zitoun, Z. Phys. C **43** (1989) 469
10. S. Brandt et al., Phys. Lett. **12** (1964) 57; E. Fahri, Phys. Rev. Lett. **39** (1977) 1587
11. Mark J Collab., D. P. Barber et al., Phys. Rev. Lett. 43 830 (1979); Mark J Collab., D. P. Barber et al., Phys. Lett. 89b, 139 (1979)
12. R.K. Ellis, D.A. Ross, A.E. Terrano: Nucl. Phys. B **178** (1981) 421; G. Parisi: Phys. Lett. B **74** (1978) 65; J.F. Donohue, F.E. Low, S.Y. Pi: Phys. Rev. D **20** (1979) 2759
13. S. Catani, G. Turnock, B. R. Webber, Phys. Lett. B295, 269 (1992)
14. S. Bethke et al., Nucl. Phys. B **370** (1992) 310
15. JADE collab., W. Bartel et al., Z. Phys. C **33** (1986); JADE collab., S. Bethke et al., Phys. Lett. B **213** (1988) 235; S. Catani, M. Seymour, Nucl. Phys. B **485** (1997) 291-419
16. Y.L. Dokshitzer, in Workshop on Jet Studies at LEP and HERA, Durham 1990, see J. Phys. G **17** (1991) 1572; S. Catani et al., Phys. Lett. B **269** (1991) 432; N. Brown, W.J. Stirling, Z. Phys. C **53** (1992) 629; S. Bethke et al., Nucl. Phys. B **370** (1992) 310
17. Yu. L. Dokshitzer et al., JHEP **08** (1998) 001
18. C. L. Basham et al., Phys. Rev. Lett. **41** (1978) 1585; C. L. Basham et al., Phys. Rev. D **17** (1978) 2298
19. Y. Ohnishi, H. Masuda, SLAC-PUB-6560 (1994); see also SLD Collab., K. Abe et al., Phys. Rev. D **51** (1995) 962

20. L. Lönnblad, Comp. Phys. Comm. **71** (1992) 15
21. G. Marchesini et al., Comp. Phys. Comm. **67** (1992) 465
22. DELPHI Collab., P. Abreu et al., Z. Phys. C **73** (1996) 11
23. HEPDATA database, URL: http://durpdg.dur.ac.uk/HEPDATA/REAC
24. S. Hahn, J. Drees, DELPHI 99-140 PHYS 827
25. W. de Boer, H. Fürstenau, J.H. Köhne, Z. Phys. C **49** (1991) 141
26. program EVENT2, M. Seymour, URL: http://hepwww.rl.ac.uk/theory/seymour/nlo
27. P. N. Burrows, H. Masuda, Z. Phys. C **63** (1994), 235-240
28. J. Chýla, A. L. Kataev, hep-ph/9502383
29. OPAL Collab., P.D. Acton et al., Z. Phys. C **55** (1992) 1
30. ALEPH Collab., D. Decamp et al., Phys. Lett. B **284** (1992) 1; L3 Collab., O. Adriani et al., Phys. Lett. B **284** (1992) 471; SLD Collab., K. Abe et al., Phys. Rev. D **51** (1995) 962
31. P. M. Stevenson, Phys. Rev. D **23** (1981) 2916
32. G. Grunberg, Phys. Rev. D **29** (1984) 2315
33. S. J. Brodsky, G.P. Lepage, P. B. Mackenziee, Phys. Rev. D **28** (1983) 228
34. N. Magnussen, Thesis, Universität Wuppertal, WUB-DIS 88-04 (1988), DESY F22-89-01; S. Bethke, Z. Phys. C **43** (1989) 331; DELPHI Collab., P. Abreu et al., Phys. Lett. B **247** (1990) 167; DELPHI Collab., P. Abreu et al., Phys. Lett. B **252** (1990) 149; JADE Collab., N. Magnussen et al., Z. Phys. C **49** (1991) 29; OPAL Collab., M.Z: Akrawy et al., Z. Phys C **49** (1991) 384; P.N. Burrows, H. Masuda, D. Muller, Phys. Lett. B **382** (1996) 157
35. Particle Data Group, Eur. Phys. J. C **3** (1998), 1
36. M. Schmelling, Phys. Scripta **51** (1995) 676
37. S. Bethke, hep-ex/9812026
38. G. Kramer, B. Lampe, Z. Phys. C **39** (1988) 101
39. M. A. Samuel, G. Li, E. Steinfels, Phys. Rev. D **48** (1993) 228; M. A. Samuel, G. Li, E. Steinfels, Phys. Rev. **E51** (1995) 3911
40. J. Ellis et al., CERN-TH/97-267 and references therein
41. J. Ellis, private communication
42. S. Catani et al., Phys. Lett. B **263** (1991) 491
43. S. Catani, B. R. Webber, Phys. Lett. B **427** (1998) 377
44. S. Catani et al., Phys. Lett. B **295** (1992) 269
45. S. Catani et al., Phys. Lett. B **272** (1991) 368
46. G. Dissertori, M. Schmelling, Phys. Lett. B **361** (1995) 167
47. Yu. L. Dokshitzer et al., JHEP **01** (1998) 011
48. S. Catani et al., Nucl. Phys. B **407** (1993) 3
49. B. R. Webber, in Proceedings of the Workshop "QCD - 20 years later", Aachen, Germany, 1992 (Word Scientific, Singapore, 1993) p 73
50. G. Rodrigo, A. Santamaria, M. Bilenky, hep-ph/9812433
51. S. Hahn, J. Drees, DELPHI 98-84 CONF 152, ICHEP'98 #142; S. Hahn, DELPHI 98-174 PHYS 813, hep-ex/9812021, Plenary talk presented at the Hadron Structure'98, Stara Lesna, Sept. 1998
52. Program provided by G. Rodrigo
53. C.T.H. Davies et al., Phys. Rev. D **56** (1997) 2755
54. J. Santiago, F. J. Ynduráin, Nucl. Phys. B **563** (1999) 45
55. The LEP Collaborations ALEPH, DELPHI, L3, OPAL, the LEP Electroweak Working Group and the SLD Heavy Flavour and Electroweak Groups, D. Abbanneo et al., CERN-EP/99-15 (1999)
56. Opal Collab., K. Ackerstaff et al., Eur. Phys. J. C **7** (1999) 571